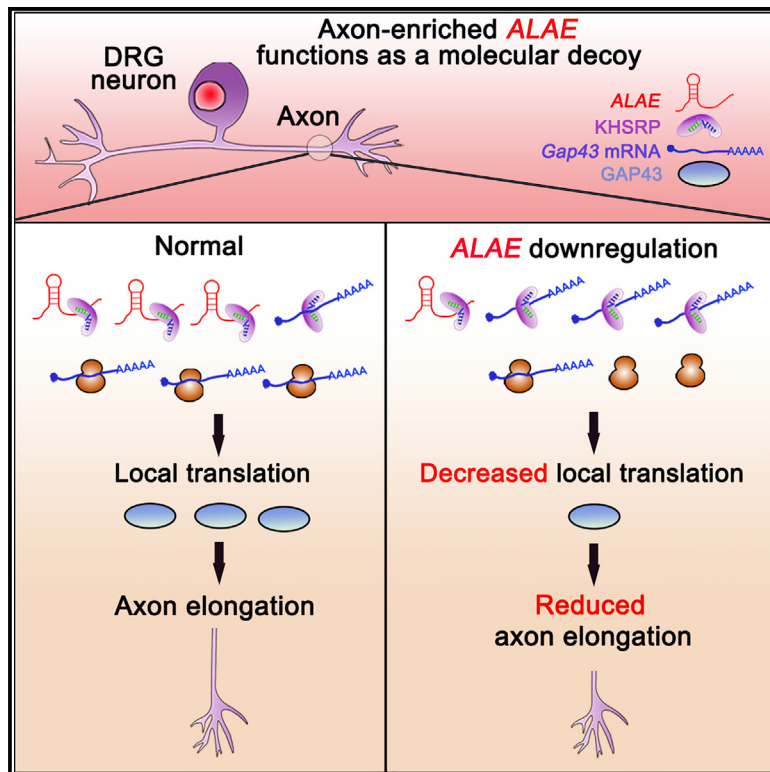


### Axon-enriched lincRNA ALAE is required for axon elongation via regulation of local mRNA translation

#### Graphical abstract



#### Authors

Manyi Wei, Jiansong Huang,  
Guo-Wei Li, ..., Li Yang, Lan Bao,  
Bin Wang

#### Correspondence

baolan@sibcb.ac.cn (L.B.),  
bin\_wang2020@163.com (B.W.)

#### In brief

Wei et al. show that lincRNA ALAE interacts with KHSRP and acts as a decoy to locally prevent translational suppression of GAP43 in axons, maintaining protein synthesis and subsequent axon elongation. The findings provide insights into how axon-enriched lincRNAs spatiotemporally orchestrate local translation of mRNAs during axon development.

#### Highlights

- ALAE is an axon-enriched lincRNA required locally for axon elongation
- ALAE interacts with the KH3–4 domains of KHSRP through AU-rich elements
- ALAE acts as a RNA decoy to prevent translational repression of KHSRP on Gap43
- Impaired ALAE-KHSRP interaction locally inhibits Gap43 translation and axon elongation



## Article

# Axon-enriched lincRNA ALAE is required for axon elongation via regulation of local mRNA translation

Manyi Wei,<sup>1,3,9</sup> Jiansong Huang,<sup>1,3,4,9</sup> Guo-Wei Li,<sup>3,5</sup> Bowen Jiang,<sup>1,3</sup> Hong Cheng,<sup>3,6</sup> Xiaoyan Liu,<sup>7</sup> Xingyu Jiang,<sup>7</sup> Xu Zhang,<sup>2,3,8</sup> Li Yang,<sup>3,5</sup> Lan Bao,<sup>1,3,4,\*</sup> and Bin Wang<sup>1,2,10,\*</sup>

<sup>1</sup>State Key Laboratory of Cell Biology, Shanghai Institute of Biochemistry and Cell Biology, CAS Center for Excellence in Molecular Cell Science, Chinese Academy of Sciences, University of the Chinese Academy of Sciences, Shanghai, China

<sup>2</sup>Shanghai Research Center for Brain Science and Brain-Inspired Intelligence, Shanghai, China

<sup>3</sup>University of Chinese Academy of Sciences, Beijing, China

<sup>4</sup>School of Life Science and Technology, ShanghaiTech University, Shanghai, China

<sup>5</sup>CAS Key Laboratory of Computational Biology, Shanghai Institute of Nutrition and Health, Chinese Academy of Sciences, Shanghai, China

<sup>6</sup>State Key Laboratory of Molecular Biology, Shanghai Institute of Biochemistry and Cell Biology, CAS Center for Excellence in Molecular Cell Science, Chinese Academy of Sciences, Shanghai, China

<sup>7</sup>Southern University of Science and Technology, Shenzhen, China

<sup>8</sup>Shanghai Advanced Research Institute, Chinese Academy of Sciences, Shanghai, China

<sup>9</sup>These authors contributed equally

<sup>10</sup>Lead contact

\*Correspondence: baolan@sibcb.ac.cn (L.B.), bin\_wang2020@163.com (B.W.)

<https://doi.org/10.1016/j.celrep.2021.109053>

## SUMMARY

Long intergenic noncoding RNAs (lincRNAs) are critical regulators involved in diverse biological processes. However, the roles and related mechanisms of lincRNAs in axon development are largely unknown. Here we report an axon-enriched lincRNA regulating axon elongation, referred to as ALAE. Profiling of highly expressed lincRNAs detected abundant and enriched ALAE in the axons of dorsal root ganglion (DRG) neurons, where it locally promoted axon elongation. Mechanically, ALAE directly interacted with the KH3–4 domains of KH-type splicing regulatory protein (KHSRP) and impeded its association with growth-associated protein 43 (Gap43) mRNA. Knockdown of ALAE reduced the protein but not the mRNA level of GAP43 in the axons of DRG neurons. Furthermore, local disruption of the interaction between ALAE and KHSRP in the axon significantly inhibited Gap43 mRNA translation, impairing axon elongation. This study implies crucial roles of axon-enriched lincRNAs in spatiotemporal regulation of local translation during axon development.

## INTRODUCTION

Neurons are highly complex cells extending long axons to their targets. During early development of the nervous system, neurons project growing axons to navigate over a long distance into the appropriate place to form functional circuits (Cioni et al., 2018). Accumulating evidence strongly supports that thousands of messenger RNAs (mRNAs) are targeted especially to developing and mature axons (Briese et al., 2016; Gumi et al., 2011). Local translation of these mRNAs is important for axon pathfinding, guidance, elongation, and survival (Cioni et al., 2018; Kar et al., 2018). Large-scale *in vivo* analysis of the axonal transcriptome suggests that locally synthesized proteins could be regulated developmentally (Shigeoka et al., 2016). Some small non-coding RNAs, microRNAs (miRNAs), have been reported to localize in the axon and regulate translation of mRNAs, affecting axon branching and elongation (Dajas-Bailador et al., 2012; Hancock et al., 2014; Wang and Bao, 2017; Wang et al., 2015).

Besides mRNAs and miRNAs, whether other types of RNAs, such as long intergenic noncoding RNAs (lincRNAs), are also localized in the axon to regulate its development remains unknown. Exploring more events mediated by other types of RNAs will help us to better understand selective control and coordination of axonal mRNA translation during neuronal development.

lincRNAs are a class of long noncoding RNAs (lncRNAs) longer than 200 nt that are transcribed from intergenic regions and lack the ability to translate into proteins. Recent studies have suggested that lncRNAs are functional as a pivotal class of modulators involved in multiple biological processes (Yao et al., 2019). Bioinformatics analysis of RNA sequencing (RNA-seq) data indicates that the majority of lincRNAs exhibit remarkable tissue specificity, such as being highly enriched in the brain and nerves (Cabili et al., 2011; Ransohoff et al., 2018). Recent studies have provided important evidence supporting crucial roles of lincRNAs, including *Pnky* and *TUNA* in neural differentiation at the early stage of brain development



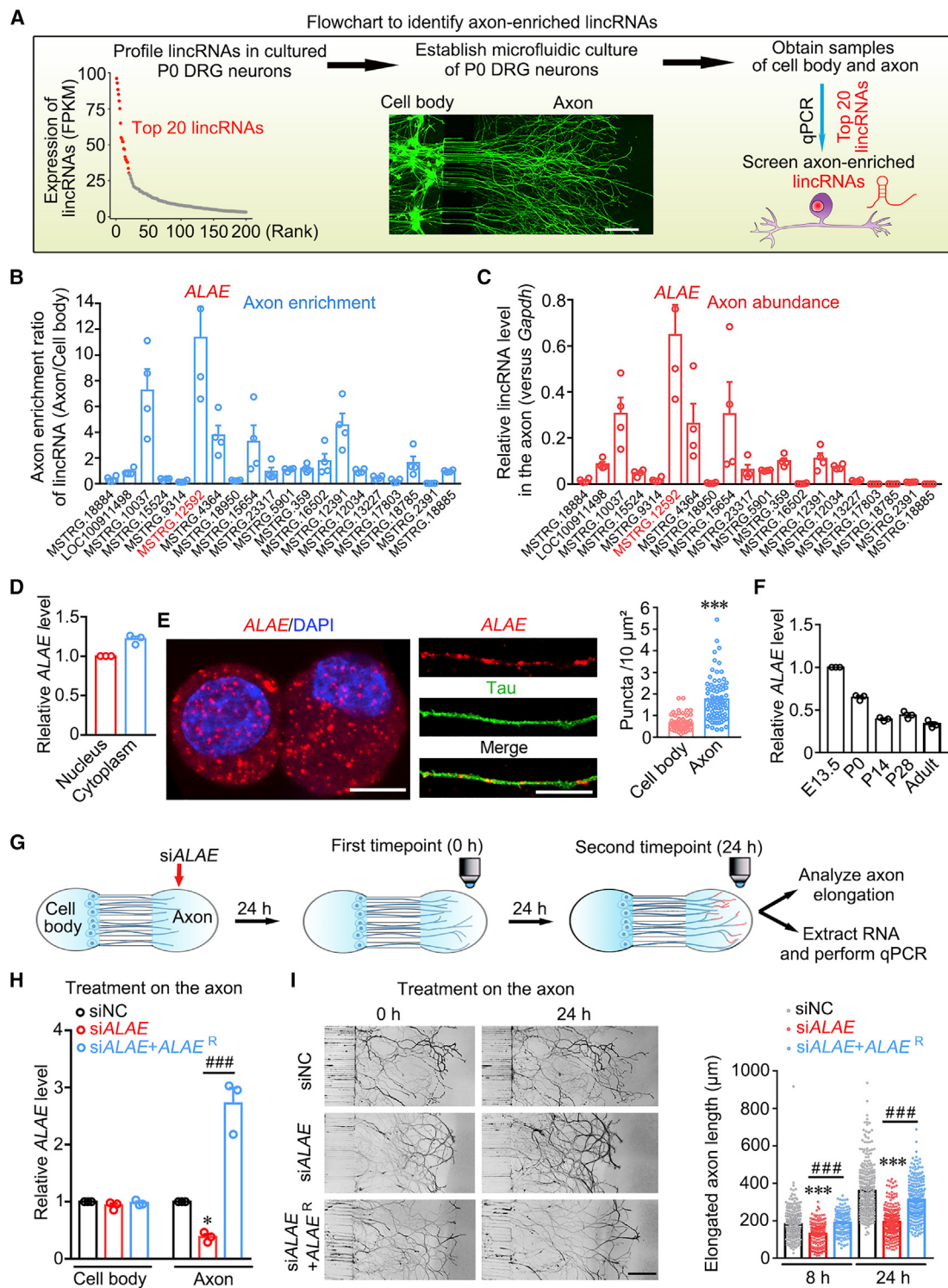


**Figure 1. Axon-enriched ALAE locally regulates axon elongation**

(A) Research flowchart for characterization of axon-enriched lncRNAs in microfluidic-cultured P0 DRG neurons. The top 200 lncRNAs were ranked by their expression levels (left). Red point, the top 20 abundant lncRNAs. The representative image shows microfluidic-cultured P0 DRG neurons at 7 days (center). Scale bar, 300  $\mu$ m.

(B and C) qPCR analysis showed that the level of ALAE in the axons was more than 10-fold higher versus that in the cell bodies (B) and that ALAE was most abundant in the axons among the top 20 highly expressed lncRNAs (C). n = 3.

(legend continued on next page)

(Lin et al., 2014; Ramos et al., 2015) and *Silc1* in peripheral neuroregeneration (Perry et al., 2018). Although lncRNAs have been demonstrated to affect neural differentiation for early development of the nervous system (Briggs et al., 2015), few have been reported to function in the late stage of neuronal development, such as axon elongation.

Localization of lncRNAs has been found to determine their functions. The majority of studied lncRNAs have been shown to be nucleus-restricted regulators for gene transcription and chromatin structure (Carlevaro-Fita and Johnson, 2019). Whether lncRNAs are distributed spatiotemporally in the axon and the roles of lncRNAs in developing axons remains unknown. In the present study, by utilizing compartmental culture of dorsal root ganglion (DRG) neurons at post-natal day 0 (P0), we identified an axon-enriched lncRNA required for axon elongation by locally regulating translation of growth-associated protein 43 (*Gap43*) mRNA, referred to as *ALAE* (axon-enriched lncRNA regulating axon elongation). Mechanistically, *ALAE* was demonstrated to act as a RNA decoy through its AU-rich element (ARE) to prevent binding and translational repression of KH-type splicing regulatory protein (KHSRP) on *Gap43* mRNA. Importantly, local disruption of the interaction between *ALAE* and KHSRP in axons significantly increased binding and translational repression of KHSRP on *Gap43* mRNA, resulting in impaired axon elongation. These findings reveal a regulatory role of lncRNAs in spatiotemporal control of mRNA translation during axon development.

## RESULTS

### ***ALAE* is an axon-enriched lncRNA in DRG neurons**

To find axon-enriched lncRNAs in DRG neurons, we first performed high-throughput RNA-seq of cultured rat DRG neurons at P0 to profile lncRNAs (Figure S1A). Briefly, sequenced fragments were aligned to the rat genome and then used to construct transcript assembly using StringTie (Pertea et al., 2015). Multi-exon transcripts without overlap with known non-lncRNA transcripts in Ensembl and RefSeq were selected. The coding potential of transcripts was estimated based on predictions from computational tools, including CPAT (Wang et al., 2013), CPC2 (Kang et al., 2017) and Pfam (El-Gebali et al., 2019) (Figure S1B). Transcripts with coding potential were removed as “putative coding.” Among 3,101 identified lncRNAs, 462 were highly expressed with fragments per kilobase of transcript per million mapped reads (FPKM) above 1 (Figures S1B and S1C;

Table S1). Those highly expressed lncRNAs exhibited a median level of 2.6 FPKM, nearly half the level of mRNA (5.8 FPKM), whereas non-highly expressed lncRNAs were expressed at a median level of 0.5 FPKM and were not considered for our further analyses (Figure S1D). Then microfluidic-cultured P0 DRG neurons was established to examine the relative expression of the top 20 lncRNAs in the cell bodies and axons of DRG neurons (Wang et al., 2015; Figures 1A). Quantitative PCR (qPCR) showed that a lncRNA, *MSTRG.12592*, called *ALAE* in the present study, was highly enriched in the axons versus the cell bodies and ranked first among tested lncRNAs (Figures 1B and S1F). Notably, *ALAE* was also the most abundant among tested lncRNAs in axons, with axon abundance equivalent to the axon growth-related transcripts *Gap43* and calmodulin (*Calm1*) (Figures 1C and S1G). Significantly, the enrichment of *ALAE* in axons was much higher than that of *Gap43* and *Calm1* mRNAs (Figure S1H). Thus, *ALAE* is a highly abundant and enriched lncRNA in the axons of DRG neurons.

The full length of *ALAE* containing 371 nt was obtained by 5' rapid amplification of cDNA ends (RACE) and 3' RACE (Figures S1I and S1J). Analysis with CPC2 software showed that *ALAE* did not have a coding ability like other known lncRNAs, such as *Miat* and *Fendrr* (Figure S2A). To evaluate the coding potential of *ALAE*, we constructed and expressed *ALAE*-GFP and GFP-*ALAE* in HEK293 cells. Immunoblotting of GFP-*ALAE* showed a similar molecular weight as GFP, and the image of *ALAE*-GFP did not exhibit any fluorescence signals, suggesting that *ALAE* might not encode a protein (Figures S2B and S2C). These data suggest that *ALAE* is indeed a lncRNA.

To further study the expression specificity of *ALAE*, we separated P0 DRG neurons from non-neuronal cells with Percoll gradients (Figure S2D). qPCR showed that *ALAE* was highly enriched in the neuronal fraction expressing *Gap43* mRNA, a neuronal marker, but not in the non-neuronal fraction expressing myelin basic protein (*Mbp*) mRNA, a Schwann cell marker (Figure S2E). Furthermore, subcellular localization of *ALAE* in DRG neurons was detected by biochemical and morphological assays. Biochemical fractionation of cultured P0 DRG neurons showed that *ALAE* was distributed similarly in the nucleus and cytoplasm (Figures 1D and S2F). This distribution pattern was confirmed by single-molecule fluorescence *in situ* hybridization (smFISH) in the cell bodies and axons of cultured P0 DRG neurons (Figure 1E). Analysis of punctum intensity showed that axonal *ALAE* was more enriched than in the cell bodies, consistent with the qPCR result (Figure 1E). The specificity of the

(D) qPCR analysis showed that *ALAE* was distributed in the nucleus and cytoplasm of P0 DRG neurons. n = 3.

(E) Representative images of smFISH (left) and quantitative data (right) showed that *ALAE* (red) was relatively enriched in the axons of cultured P0 DRG neurons. DAPI (blue) was used to indicate the nucleus. Tau (green) was used to indicate the axon profile. Scale bar, 10 μm. Cell bodies, n = 60; axons, n = 79. \*\*\*p < 0.001 versus cell body.

(F) qPCR analysis showed that expression of *ALAE* decreased progressively in DRGs from E13.5 to P14 and then stayed at a certain level to adulthood. n = 3.

(G) Research flowchart for detection of axon elongation in the microfluidic chamber.

(H) qPCR analysis showed expression of *ALAE* in the cell bodies and axons after knockdown or coexpression of *ALAE*<sup>R</sup> in the axons of DRG neurons. siNC, negative control. n = 3. \*p < 0.05 versus siNC and #\*\*\*p < 0.001 versus the indicated treatment.

(I) Representative images (left) and quantitative data (right) showed that knockdown of *ALAE* in the axons reduced axon elongation and coexpression of *ALAE*<sup>R</sup> in the axons largely rescued the decreased axon elongation. 8 h: siNC, n = 290; si*ALAE*, n = 164; si*ALAE*+*ALAE*<sup>R</sup>, n = 139; 24 h: siNC, n = 342; si*ALAE*, n = 259; si*ALAE*+*ALAE*<sup>R</sup>, n = 254. \*\*\*p < 0.001 versus siNC and #\*\*\*p < 0.001 versus the indicated treatment.

The results are presented as mean ± SEM.

See also Figures S1–S3 and Table S1.

smFISH signal was confirmed by utilizing *Dapb*, a bacterial gene, as a negative control (Figure S2G) and short hairpin RNA (shRNA)-mediated knockdown of *ALAE* in cultured P0 DRG neurons (Figures S2H and S2I). Therefore, *ALAE* is an abundant lincRNA localized in the axons of DRG neurons.

The conservation of lincRNAs among species suggests their importance during the evolutionary process. Then we analyzed the conservation of *ALAE* by VISTA browser and BLAST analysis. *ALAE* is localized genomically downstream of *Prss12* with opposite direction as a spliced, polyadenylated, and conserved lincRNA with a length of 371, 448, and 619 nt in rat, mouse, and human, respectively (Figure S2J). The orthologs of *ALAE* in human and mouse are *SNHG8* and *Snhg8*, respectively. Moreover, the rat *ALAE* sequence is 71% similar to that of mouse *Snhg8* and 38% similar to that of human *SNHG8* (Figure S2K). Thus, *ALAE* is a conserved lincRNA among rodents and humans.

### ***ALAE* is required for axon elongation in the axons of DRG neurons**

Developmental expression of *ALAE* was detected during DRG development. qPCR showed that the level of *ALAE* was high at embryonic day 13.5 (E13.5) and P0, important periods for rapid axon growth of DRG neurons, and decreased in the following stages (Figure 1F). This expression pattern raises the possibility that axon-enriched *ALAE* functions during axon development. Then we examined axon elongation after selective knockdown of *ALAE* with small interfering RNA (si*ALAE*) in the axon compartment (Figure 1G). Application of si*ALAE* in the axon compartment selectively reduced *ALAE* in axons but not cell bodies, and coexpression of small interfering RNA (siRNA)-resistant *ALAE* (*ALAE*<sup>R</sup>) completely rescued the decreased level of *ALAE* (Figure 1H). After siRNA treatment for 24 h, the length of the elongated axons was traced and measured for 8 h and 24 h (Figure 1G). Importantly, knockdown of *ALAE* in the axon compartment reduced the axon elongation rate, whereas coexpression of *ALAE*<sup>R</sup> mostly rescued decreased axon elongation because of si*ALAE* treatment (Figure 1I). *ALAE* siRNA was also transfected into the cell body compartment of microfluidic-cultured P0 DRG neurons, and the length of the elongated axons was traced and measured for 24 h (Figure S3A). As expected, the level of *ALAE* was reduced significantly in cell bodies and axons of DRG neurons, and these reduced levels were rescued completely by coexpression of *ALAE*<sup>R</sup> (Figure S3B). Knockdown of *ALAE* in the cell body compartment also resulted in decreased axon elongation, which was rescued fully by *ALAE*<sup>R</sup> coexpression (Figure S3C). Comparable effects on axon elongation by knockdown of *ALAE* in the cell body and axon compartments (Figures 1H, 1I, S3B, and S3C) imply that *ALAE* plays a prominent role in the axon. In addition, to evaluate the effect of *ALAE* overexpression on axon elongation, we electroporated pcDNA-*ALAE* in the cell body compartment of microfluidic-cultured P0 DRG neurons and the length of the elongated axons were also traced and measured for 24 h. Although qPCR showed that *ALAE* was increased significantly in cell bodies and axons (Figure S3D), axon elongation was not affected by overexpression of *ALAE* (Figure S3E), implying a possible intrinsic mechanism of *ALAE* effects because of its abundance in axons. These

results suggest that axon-enriched *ALAE* is required for axon elongation in DRG neurons.

### ***ALAE* associates with KHSRP through AREs in DRG neurons**

Because *ALAE* displayed a significant role in axon elongation, we next sought to explore the underlying molecular mechanisms. We speculated that *ALAE* might exert this role by binding and affecting the function of some important proteins. To examine this possibility, RNA pull-down was performed by using biotinylated sense and antisense (negative control) transcripts of *ALAE* in pheochromocytoma 12 (PC12) cells, which express a similar level of *ALAE* as cultured P0 DRG neurons (Figures 2A and S4A). Analysis of mass spectrometry detected that two RNA-binding proteins (RBPs), KHSRPs and far upstream element binding protein 1 (FUBP1), ranked the highest based on enrichment by *ALAE* sense versus antisense (Figure 2B; Table S2). Immunoblotting confirmed that KHSRP and FUBP1, but not the neuronal RBP HuD, were pulled down specifically by *ALAE* sense in PC12 cells and P0 DRGs (Figures 2C, S4B, and S4C). Furthermore, RNA immunoprecipitation (RIP) using antibodies of endogenous proteins followed by qPCR showed that *ALAE* was apparently present in the immunoprecipitates of KHSRP and FUBP1, but not that of HuD, in PC12 cells and P0 DRGs (Figures 2D–2F). A previous study showed that FUBP1 was localized primarily in the nucleus of neurons and involved in neural differentiation (Hwang et al., 2018). We carried out immunostaining of FUBP1 in cultured P0 DRG neurons and found that FUBP1 was restricted to the nucleus of the cell body (Figure S4D). Therefore, we focused on KHSRP as an *ALAE*-associated protein in the axons of DRG neurons. Consistent with *ALAE* association with KHSRP in DRG neurons, co-staining of KHSRP with *ALAE* in cultured P0 DRG neurons showed that approximately 8% and 18% of *ALAE*-positive granules contained KHSRP, and approximately 8% and 13% of KHSRP-positive granules contained *ALAE* in the cell body and axon, respectively (Figure 2H). Given the highly efficient binding of KHSRP with *ALAE* seen by RIP (Figure 2F), we speculated that morphological detection of co-localization in granules might underestimate the interaction between KHSRP and *ALAE*. Therefore, *ALAE* associates with KHSRP in DRG neurons.

To determine which part of *ALAE* is responsible for its interaction with KHSRP, we used 3 fragments of *ALAE*, 1–150 nt, 1–222 nt, and 223–371 nt, to perform RNA pull-down in P0 DRGs. Immunoblotting showed that the fragment of 223–371 nt interacted efficiently with KHSRP (Figure 3A). Further mapping revealed that deletion of the fragment of 318–351 nt, but not 223–261 nt, 262–317 nt, and 352–371 nt, impaired *ALAE* interaction with KHSRP (Figure 3B). Because the K homology (KH) domain is essential for protein binding with RNAs (Gherzi et al., 2004), we compared the binding ability for the full-length and (KH1–4) of KHSRP on *ALAE* in cultured HEK293 cells without endogenously expressing *ALAE* (Figure S4E). Immunofluorescence images showed that KH1–4-GFP localized mainly in the cytoplasm because of the absence of a nuclear localization signal (NLS) (Gherzi et al., 2010), whereas most of KHSRP-GFP was in the nucleus (Figure 3C). Obviously, the amount of exogenous KHSRP in HEK293 cells was more prone to localize

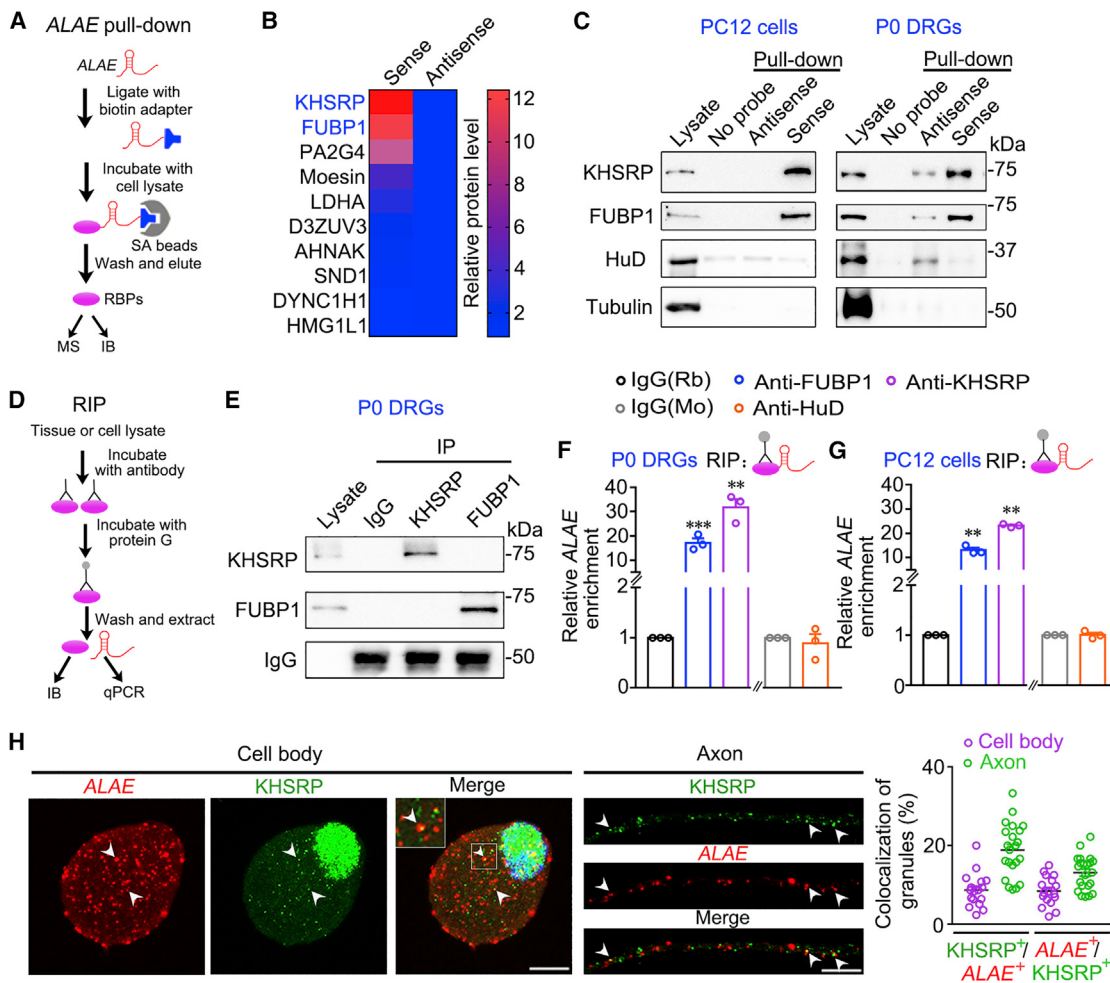


**Figure 2. ALAE interacts with KHSRP**

(A) Flowchart for the biotin-labeled RNA pull-down assay combined with mass spectrometry (MS) to identify ALAE-associated proteins. IB, immunoblotting.

(B) Heatmap showing ALAE-associated proteins.

(C) Representative immunoblots showed that KHSRP and FUBP1 were pulled down by biotinylated ALAE in PC12 cells (left) and P0 DRG tissues (right). HuD and tubulin served as negative controls.

(D) Flowchart for RNA immunoprecipitation (RIP) experiments combined with qPCR to detect protein-associated ALAE in cultured PC12 cells and P0 DRG tissues.

(E) Representative immunoblots showing the products of immunoprecipitation (IP) by KHSRP and FUBP1 in P0 DRGs. Immunoglobulin G (IgG) served as a control.

(F and G) qPCR analysis showed that ALAE was abundant in the KHSRP immunoprecipitates of P0 DRG tissues (F) and PC12 cells (G). n = 3. \*\*p < 0.05, \*\*\*p < 0.001 versus IgG.

(H) Representative images (left) and quantitative data (right) showed that ALAE (red) was co-localized with KHSRP (green) in the cell bodies and axons of cultured P0 DRG neurons. Cell bodies, n = 17; axons, n = 22. Scale bar, 10 μm.

The results are presented as mean ± SEM.

See also Figure S4 and Table S2.

in the nucleus than that in DRG neurons (Figure 2H), likely because of a lack of important molecules to keep KHSRP in the cytoplasm of HEK293 cells. qPCR showed that the amount of exogenous ALAE was more enriched in the immunoprecipitate of KH1–4-GFP-FLAG compared with KHSRP-GFP-FLAG (Figures 3D, 3E, and S4F), suggesting that KH1–4 is better suited for screening the interaction region of ALAE with KHSRP. Furthermore, the amounts of ALAEΔ223–371 and ALAEΔ318–351 were decreased dramatically compared with the full-length

ALAE in the immunoprecipitates of KH1–4-GFP-FLAG (Figures 3F and S4G). Therefore, ALAE318–351 is required for interaction of ALAE with KHSRP.

Because KHSRP has been shown to especially bind RNAs containing AREs (Gherzi et al., 2004, 2010), we noticed that the sequence of ALAE318–351 revealed 85% AU as an ARE (Figure S4H). Conservation analysis showed that the rat ALAE318–351 sequence is 75% similar to that of mouse Snhg8 and 50% similar to that of human SNHG8 (Figure S4I). In addition, the

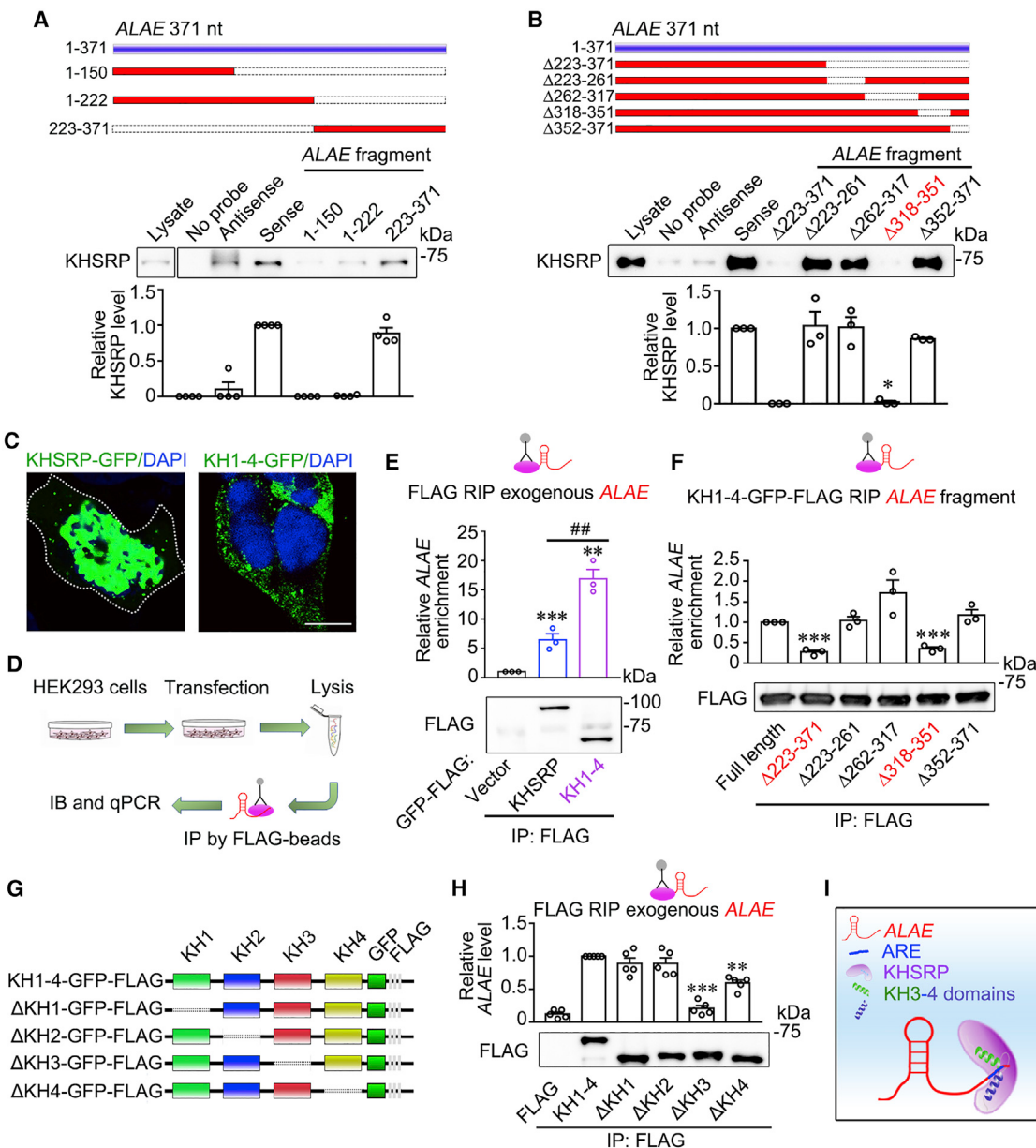


**Figure 3. The ALAE 318–351 domain is required for association with KHSRP**

(A and B) Schematic of the full-length ALAE and its fragments in the RNA pull-down assay (top). Representative immunoblots and quantitative data (down) showed that 223–271 nt (A) and 318–351 nt (B) of ALAE were required for association with KHSRP. n = 4. \*p < 0.05 versus sense.

(C) Representative images showing mainly nuclear distribution of KHSRP-GFP-FLAG and highly cytoplasmic distribution of KH1-4-GFP-FLAG in HEK293 cells. DAPI served as a nuclear marker. Scale bar, 10 μm.

(D) Flowchart for RIP experiments in cultured HEK293 cells expressing ALAE with KHSRP-GFP-FLAG or KH1-4-GFP-FLAG.

(E) qPCR analysis and representative immunoblots showed that ALAE was more abundant in FLAG immunoprecipitates of HEK293 cells expressing KH1-4-GFP-FLAG. n = 3. \*\*p < 0.01, \*\*\*p < 0.001 versus vector and #p < 0.01 versus indicated.

(F) qPCR analysis and representative immunoblots showed that 318–351 nt of ALAE were required for ALAE association with KHSRP in HEK293 cells. n = 3. \*\*\*p < 0.001 versus full-length ALAE.

(G) Schematic of KH1-4 truncations.

(H) qPCR analysis and representative immunoblots showed that the KH3–4 domains were required for KHSRP interaction with ALAE in HEK293 cells. n = 5. \*\*p < 0.01, \*\*\*p < 0.001 versus KH1-4-GFP-FLAG.

(I) A proposed model for ALAE interaction with the KH3–4 domains of KHSRP via the AREs.

The results are presented as mean ± SEM.

See also Figure S4.

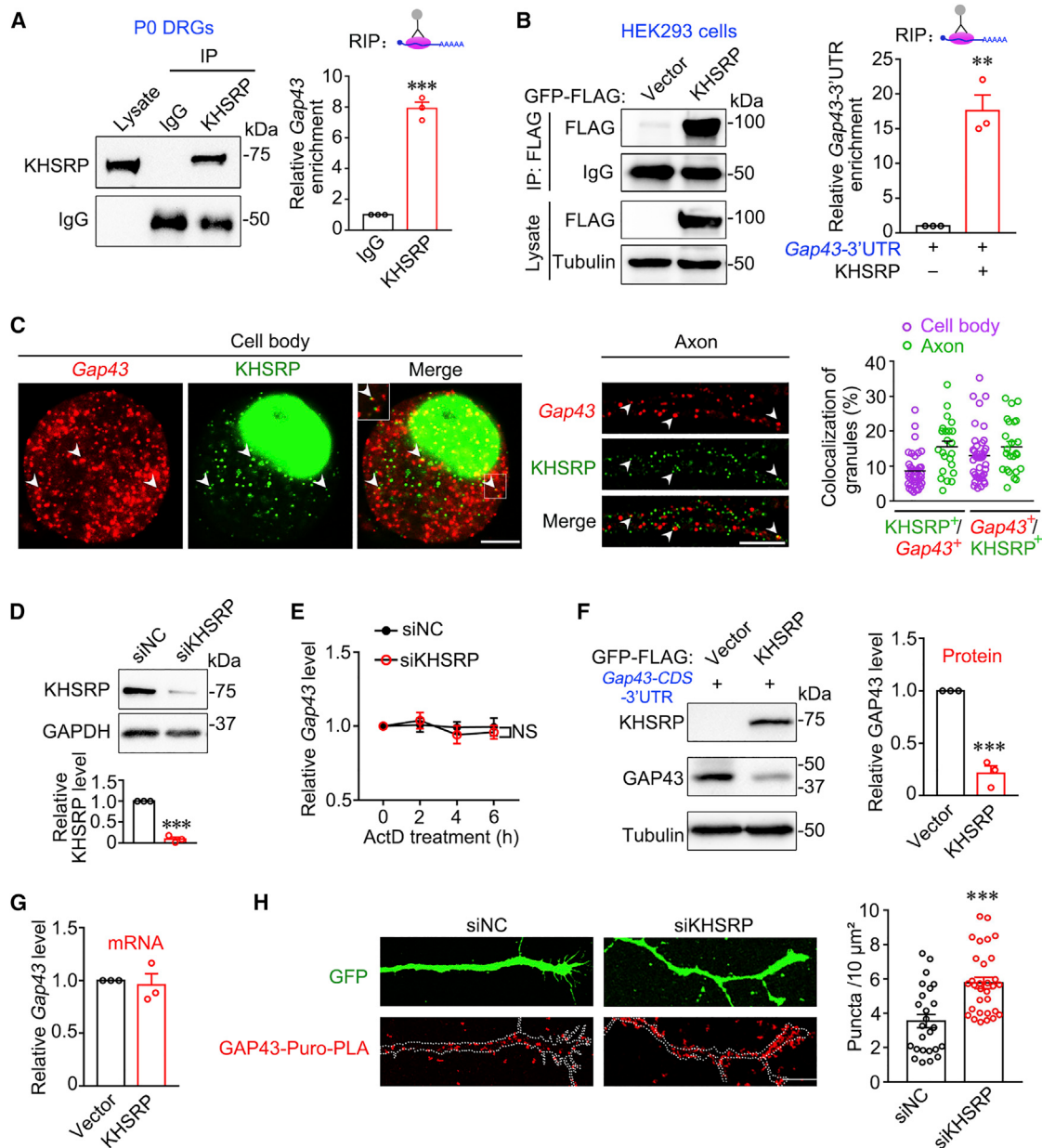


**Figure 4. KHSRP interacts and represses Gap43 mRNA translation in DRG neurons**

- (A) Representative immunoblots (left) and qPCR analysis (right) showed that *Gap43* mRNA was abundant in KHSRP immunoprecipitates of P0 DRG tissues. IgG served as a control. n = 3.
- (B) Representative immunoblots (left) and qPCR analysis (right) showed that *Gap43*-3' UTR was abundant in KHSRP-GFP-FLAG immunoprecipitates of HEK293 cells. GFP-FLAG served as a control. n = 3.
- (C) Representative images (left) and quantitative data (right) showed that *Gap43* mRNA (red) was co-localized with KHSRP (green) in the cell bodies and axons of cultured P0 DRG neurons. Cell body, n = 39; axon, n = 23. Scale bar, 10  $\mu\text{m}$ .
- (D) Representative immunoblots (top) and quantitative data (bottom) showing efficient siRNA-mediated knockdown of KHSRP in cultured P0 DRG neurons. GAPDH served as a loading control. n = 3.
- (E) qPCR analysis showed that the turnover of *Gap43* mRNA was not affected by knockdown of KHSRP in cultured DRG neurons. n = 5. Two-way ANOVA was used to examine statistical significance. NS, non-significant.
- (F) Representative immunoblots (left) and quantitative data (right) showed that the protein level of GAP43 was reduced by overexpression of KHSRP-GFP-FLAG in HEK293 cells expressing *Gap43*-CDS-3' UTR. n = 3.
- (G) qPCR analysis showed that the level of *Gap43* mRNA was not altered by overexpression of KHSRP-GFP-FLAG in HEK293 cells expressing *Gap43*-CDS-3' UTR. n = 3.

(legend continued on next page)

percentages of AU in this region are 85%, 94%, and 69% in rat, mouse, and human, respectively (Figure S4I). The conserved AREs and their enriched AU sequences suggest possible functional conservation.

To further determine the precise domain of KHSRP for interacting with ALAE, we performed RIP in HEK293 cells expressing different truncations of KH domains (Figure 3G). qPCR showed that deletion of the KH3 or KH4 domain largely reduced the amount of co-immunoprecipitated ALAE (Figures 3H and S4J). Because the truncation deleting KH3 or KH4 exhibited cytoplasmic localization similar to KH1–4-GFP, the binding difference of ALAE with KH1–4-GFP and ΔKH3 or ΔKH4 truncation was not due to their localization (Figure S4K). These results suggest that ALAE associates with the KH3–4 domains of KHSRP through AREs (Figure 3I).

### KHSRP interacts with Gap43 mRNA and represses its translation in DRG neurons

Because the role of KHSRP in stability of *Gap43* mRNA has been reported to be during axon outgrowth of embryonic hippocampal neurons (Bird et al., 2013), we next sought to examine the interaction between KHSRP and *Gap43* mRNA by a RIP experiment in P0 DRGs. qPCR showed that *Gap43* mRNA was enriched in KHSRP immunoprecipitates (Figure 4A). Association of KHSRP with the 3' untranslated region (UTR) of *Gap43* mRNA was confirmed by qPCR using a FLAG antibody in HEK293 cells coexpressing KHSRP-GFP-FLAG and *Gap43*-3' UTR (Figure 4B). Moreover, immunostaining of KHSRP combined with smFISH showed that approximately 8% and 15% of *Gap43*-positive granules contained KHSRP and 13% and 16% of KHSRP-positive granules contained *Gap43* in the cell body and axon, respectively (Figure 4C). The specificity of the smFISH signal for *Gap43* was also confirmed by the negative control for *Dapb* (Figure S5A). Therefore, KHSRP interacts with *Gap43* mRNA in DRG neurons.

To determine the effect of KHSRP on the stability of *Gap43* mRNA, we used Actinomycin D (ActD) as a transcriptional inhibitor for detecting mRNA stability after application of siKHSRP in cultured P0 DRG neurons (Figure 4D). qPCR showed that the turnover rate of *Gap43* mRNA was unaffected by knockdown of KHSRP (Figure 4E). We next examined whether KHSRP regulates the level of GAP43 protein by coexpressing GFP-Gap43-CDS-3' UTR and KHSRP-GFP-FLAG in HEK293 cells. Immunoblotting and qPCR showed that overexpression of KHSRP-GFP-FLAG decreased the protein but not mRNA level of GAP43 (Figures 4F and 4G). Although qPCR and immunoblotting detected that knockdown of KHSRP did not affect the total mRNA and protein levels of GAP43 in cultured P0 DRG neurons (Figures S5B and S5C), immunofluorescence images and quantitative results showed that the intensity of GAP43 in axons was increased after application of siKHSRP in the cell body compartment of microfluidic-cultured P0 DRG neurons (Figure S5D), implying a more sensitive effect of KHSRP repression on local

GAP43 in axons. To determine whether KHSRP affects newly synthesized GAP43 in axons, we successfully established a puromycin proximity ligation assay (puro-PLA) according to a previous study (tom Dieck et al., 2015; Figure S5E). Fluorescence images and quantitative data showed that nascent GAP43 labeling with puro-PLA in axons was increased significantly after application of siKHSRP in the cell body compartment of microfluidic-cultured P0 DRG neurons (Figure 4H), supporting translational repression of KHSRP on *Gap43* mRNA. These data suggest a regulatory role of KHSRP in repressing translation of *Gap43* mRNA.

### ALAE downregulation reduces the protein but not mRNA level of GAP43 in the axons of DRG neurons

Given a critical role of KHSRP-mediated repression on *Gap43*-3' UTR with known AREs (Yoo et al., 2013), we next investigated whether ALAE affects this effect of KHSRP. Adeno-associated virus (AAV) 2/8-mediated knockdown of ALAE was utilized in microfluidic-cultured P0 DRG neurons (Figures 5A and S5F). After 7-day infection in the cell body compartment, qPCR showed that ALAE was decreased dramatically in cell bodies and axons (Figure 5B). The amount of GAP43 protein in cell bodies and axons was decreased significantly, whereas the level of *Gap43* mRNA remained unchanged (Figures 5B and 5C), suggesting that ALAE positively affects GAP43 protein levels. In support of this possibility, immunofluorescence images showed that the intensity of GAP43 in axons was reduced in cultured P0 DRG neurons electroporated with shALAE (Figure 5D). As a control, the protein and mRNA levels of calmodulin in cell bodies and axons were not affected by knockdown of ALAE in the cell body compartment (Figures 5B and 5C). qPCR and immunoblotting showed that the mRNA and protein levels of KHSRP in cell bodies were not affected by shALAE (Figures S5G and S5H), indicating that ALAE affects GAP43 without directly through regulating KHSRP level. Furthermore, fluorescence images and quantitative data showed that nascent GAP43 labeling with puro-PLA in axons was reduced significantly after application of siALAE in cultured P0 DRG neurons (Figure 5E), confirming translational repression of ALAE on *Gap43* mRNA.

To examine the local effect of ALAE on GAP43 expression in axons, we exclusively transfected siRNA in the axon compartment of microfluidic-cultured P0 DRG neurons. qPCR showed that application of siRNA in the axon compartment reduced the axonal but not cell body level of ALAE, and coexpression of ALAE<sup>R</sup> completely rescued the amount of ALAE in axons affected by siRNA (Figure 5F). Importantly, immunoblotting showed that knockdown of ALAE in axons decreased the protein level of GAP43 without affecting its mRNA level in axons but not cell bodies (Figure 5G). However, the protein and mRNA levels of calmodulin in cell bodies and axons were not changed after knockdown of ALAE in axons (Figures 5F and 5G). The effect of whole-cell knockdown by 7-day infection with AAV-shALAE on GAP43 levels seems to be stronger in comparison with

(H) Representative images (left) and quantitative data (right) showed that knockdown of KHSRP in the cell body compartment increased newly synthesized GAP43 in axons in microfluidic-cultured P0 DRG neurons. GFP was used to indicate the axon profile. siNC, n = 25; siKHSRP, n = 31. Scale bar, 10 μm. The results are presented as mean ± SEM. \*\*p < 0.01, \*\*\*p < 0.001 versus control. See also Figure S5.

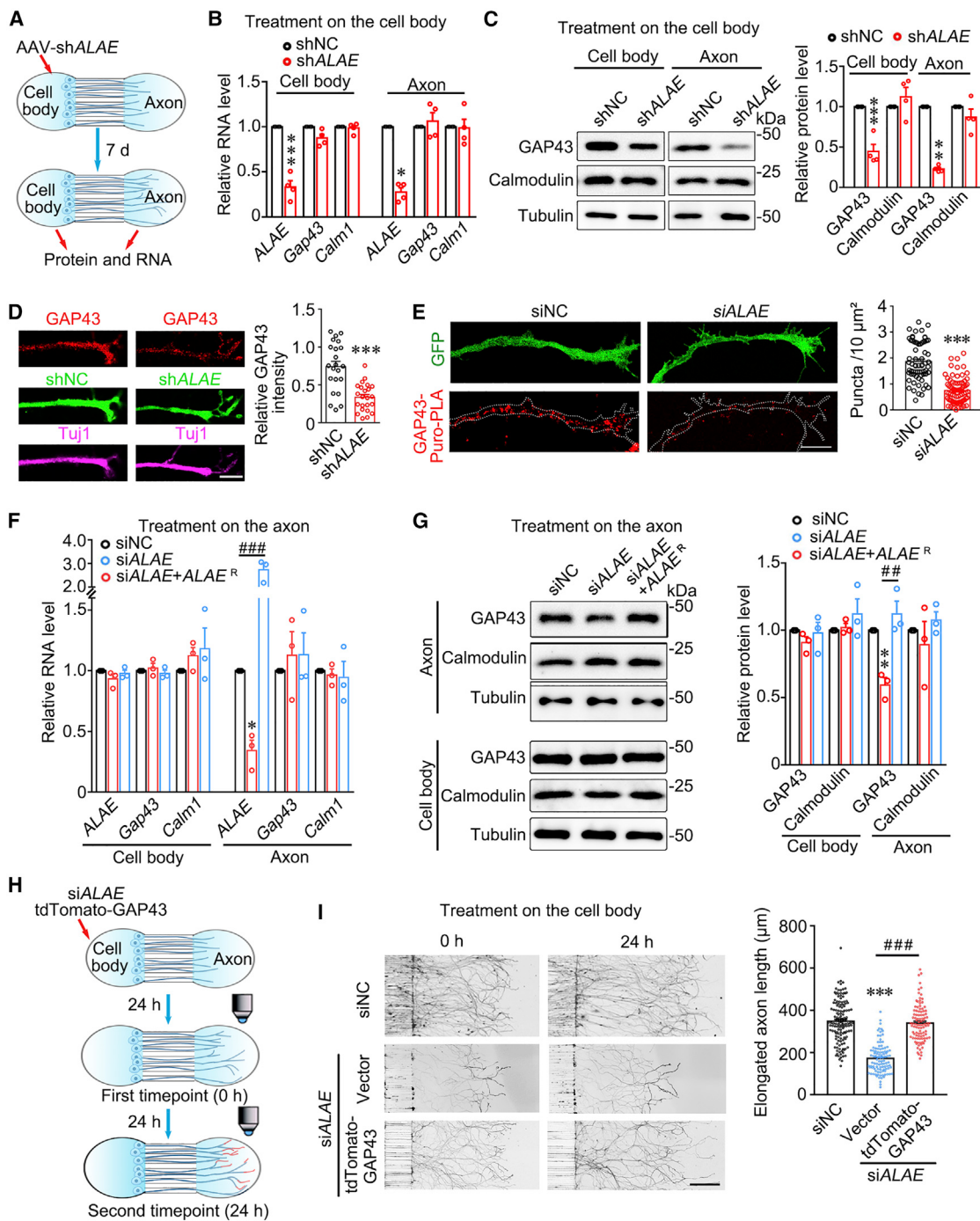


**Figure 5. ALAE downregulation reduces the level of GAP43 protein but not mRNA in the axons of DRG neurons**

(A) Flowchart for AAV-mediated knockdown of ALAE in microfluidic-cultured P0 DRG neurons.

(B) qPCR analysis showed that ALAE was decreased in cell bodies and axons by infection with AAV-shALAE, whereas Gap43 mRNA remained unchanged. Calm1 was used as a negative control. n = 4. \*p < 0.05, \*\*p < 0.01 versus shNC.

(C) Representative immunoblots (left) and quantitative data (right) showed that infection with AAV-shALAE significantly decreased the protein level of GAP43 in the cell bodies and axons of microfluidic-cultured P0 DRG neurons at 7 days *in vitro* (DIV). n = 4. \*\*p < 0.01, \*\*\*p < 0.001 versus shNC.

(D) Representative images (left) and quantitative data (right) showed that shRNA-mediated knockdown of ALAE reduced the intensity of GAP43 in the axons of cultured P0 DRG neurons. shNC, n = 22; shALAE, n = 23. \*\*\*p < 0.001 versus shNC. Scale bar, 10  $\mu\text{m}$ .

(E) Representative images (left) and quantitative data (right) showed that siALAE reduced newly synthesized GAP43 in the axons of cultured P0 DRG neurons. GFP was used to indicate the axon profile. siNC, n = 68; siALAE, n = 76. \*\*\*p < 0.001 versus siNC. Scale bar, 10  $\mu\text{m}$ .

(legend continued on next page)

siALAE for 48 h in axons, possibly because of its more stable and long-term effect silencing ALAE. We also examined whether ALAE overexpression affected the protein level of GAP43. Immunoblotting showed that the amount of GAP43 was not affected by overexpression of ALAE in the cell body compartment of microfluidic-cultured P0 DRG neurons (Figure S5I), consistent with the ineffective axon elongation by ALAE overexpression. All of these data suggest that downregulation of ALAE reduces the protein but not mRNA level of GAP43 in the axons of DRG neurons.

To determine whether GAP43 is the major downstream target for ALAE-related axon elongation, we performed an axon elongation assay after application of siALAE and coexpression of tdTomato-GAP43 in the cell body compartment of microfluidic-cultured P0 DRG neurons. Immunoblotting showed that coexpression of tdTomato-GAP43 fully rescued the decreased amounts of GAP43 by siALAE (Figure S5J). Furthermore, representative images and quantitative data showed that coexpression of tdTomato-GAP43 largely rescued the decreased axon elongation because of siALAE treatment in the axon compartment (Figure 5I), implicating GAP43 as the major target of ALAE during axon elongation. Therefore, ALAE is required for axon elongation through translational regulation of Gap43 mRNA.

#### ALAE impedes KHSRP association with Gap43 mRNA and its repression of Gap43 mRNA translation and axon elongation

To further explore the effect of ALAE on KHSRP association with Gap43 mRNA, we performed RIP in HEK293 cells coexpressing KH1–4-GFP-FLAG and Gap43-3' UTR in the absence or presence of ALAE. qPCR showed that the amount of co-immunoprecipitated Gap43-3' UTR was decreased dramatically in the presence of ALAE (Figures 6A and S6A), suggesting that ALAE competes with Gap43-3' UTR for KHSRP binding. Consistently, knockdown of ALAE in PC12 cells increased the amount of endogenous Gap43 mRNA co-immunoprecipitated by KHSRP (Figures 6B and S6B). These data suggest that ALAE interacts with KHSRP to compete the association of KHSRP with Gap43 mRNA.

To further test this possibility, we next examined whether Gap43-3' UTR and ALAE interacted with the same domain of KHSRP. We performed RIP to determine the precise domain of KHSRP interacting with Gap43 mRNA in HEK293 cells expressing different truncations of KH domains. Interestingly, deletion of the KH3 or KH4 domain reduced the amount of co-immunoprecipitated Gap43-3' UTR (Figures 6C and S6C), implying that the

KH3–4 domains are required for KHSRP association with ALAE and Gap43 mRNA. To examine whether ALAE functioned as a decoy, we performed smFISH for Gap43 combined with immunofluorescence for KHSRP after ALAE knockdown in the axon compartment of microfluidic-cultured P0 DRG neurons. The images and quantitative data showed that the percentage of co-localization between KHSRP and Gap43 mRNA was increased significantly by exclusive application of siALAE in axons (Figure 6D). To explore axonal co-localization of KHSRP with ALAE and Gap43 mRNA, we performed double smFISH for ALAE and Gap43 mRNA combined with immunostaining for KHSRP. Quantitative data showed that ALAE was localized in only 4.9% of KHSRP granules containing Gap43 (Figure S6D), implying that ALAE and Gap43 mRNA associate with distinct KHSRP granules. These results suggest a decoy mechanism of ALAE to impede interaction of KHSRP with Gap43 mRNA (Figure 6E).

To further determine the decoy effect of ALAE on KHSRP in DRG neurons, we detected axonal GAP43 levels after application of siALAE or siALAE and siKHSRP in the cell body compartment of microfluidic-cultured P0 DRG neurons. Immunofluorescence images and quantitative data showed that knockdown of KHSRP and ALAE restored the decreased intensities of newly synthesized and total GAP43 in axons (Figures 6F and S6E) as well as the defect of axon elongation (Figure 6G) because of siALAE treatment, implicating KHSRP as a major regulator participating in ALAE-mediated local translation of Gap43 mRNA. Moreover, we also examined axonal GAP43 levels in microfluidic-cultured P0 DRG neurons coexpressing KHSRP and ALAE in the cell body compartment. Immunofluorescence images and quantitative data showed that the reduced intensities of newly synthesized and total GAP43 in axons because of overexpression of KHSRP were rescued fully by coexpression of ALAE (Figures 6H and S6F). Decreased axon elongation by overexpressing KHSRP was also restored by coexpression of ALAE in the microfluidic-cultured P0 DRG neurons (Figure 6I). These results suggest that ALAE serves as a decoy on KHSRP and impedes its repression on Gap43 mRNA translation and axon elongation.

#### Disruption of the interaction between ALAE and KHSRP inhibits local translation of Gap43 mRNA and axon elongation

Because ALAE318–351 was required for interaction of ALAE with KHSRP, we designed an ALAE 318–351 sense fragment resistant to siALAE to determine its rescue effect on the reduced level of GAP43 by ALAE knockdown in cultured P0 DRG neurons.

(F) qPCR analysis showed that axonal application of siALAE decreased the level of ALAE in axons but not cell bodies of microfluidic-cultured P0 DRG neurons. The decreased level of ALAE was rescued completely by cotransfection with ALAE<sup>R</sup>. The levels of Gap43 and Calm1 mRNAs in the cell bodies and axons were not changed by the indicated treatments.

(G) Representative immunoblots (left) and quantitative data (right) showed that axonal application of siALAE decreased the level of GAP43 in the axons but not cell bodies of microfluidic-cultured P0 DRG neurons. The decreased level of GAP43 was rescued completely by cotransfection with ALAE<sup>R</sup> in axons. n = 3. \*p < 0.05, \*\*p < 0.01 versus siNC and #p < 0.01, ##p < 0.001 versus indicated.

(H) The flowchart for electroporation of the tdTomato-GAP43 rescue experiment in microfluidic-cultured P0 DRG neurons.

(I) Representative images (left) and quantitative data (right) showed that knockdown of ALAE in the cell body compartment reduced axon elongation and that coexpression of tdTomato-GAP43 in the cell body completely rescued decreased axon elongation. siNC, n = 142; siALAE, n = 108; siALAE + tdtomato-GAP43, n = 101. \*\*\*p < 0.001 versus siNC and ###p < 0.001 versus indicated.

The results are presented as mean ± SEM.

See also Figure S5.

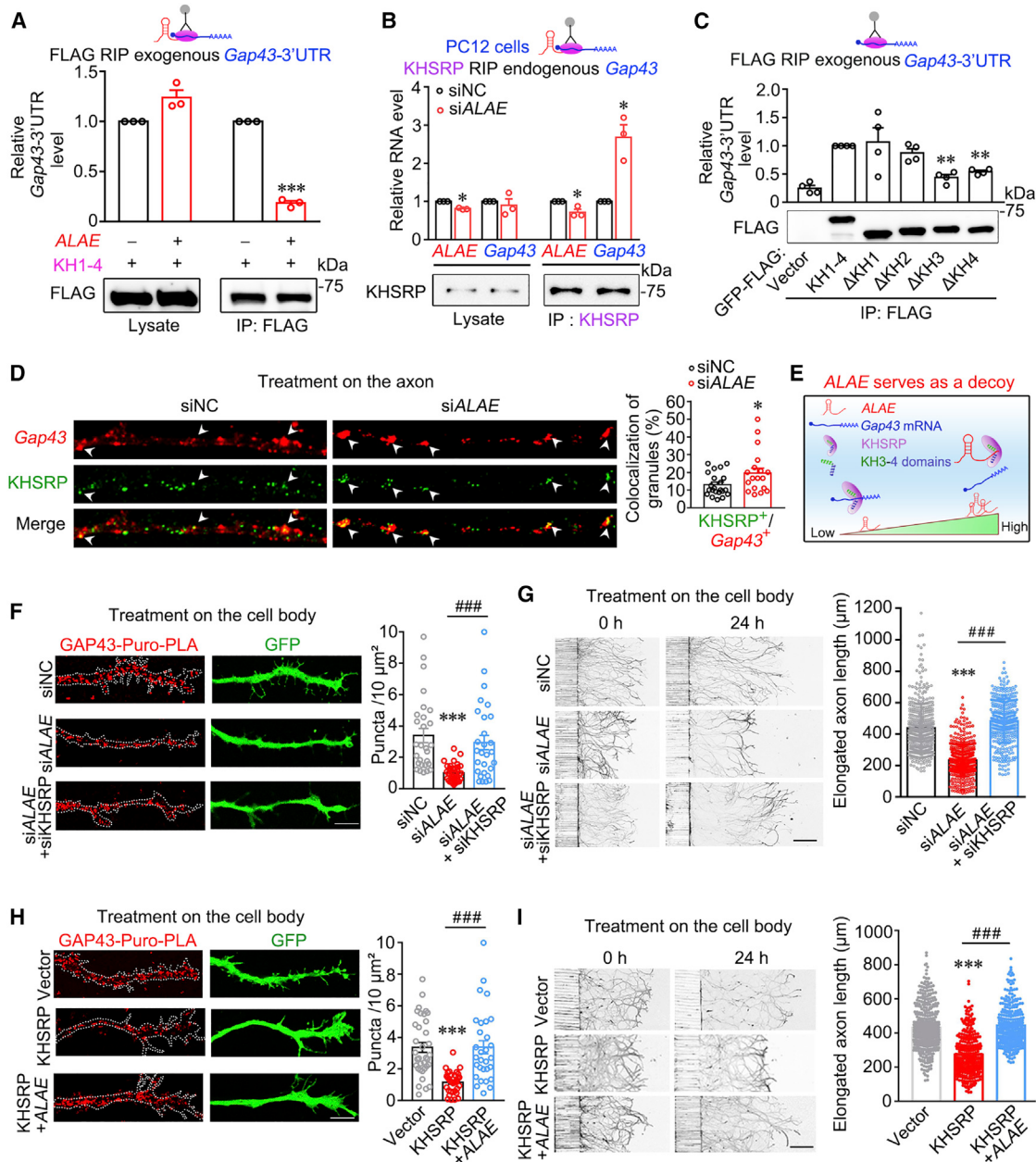


**Figure 6. ALAE competes the association of KHSRP with *Gap43*mRNA**

(A) qPCR analysis and representative immunoblots showed that association of *Gap43-3' UTR* with KHSRP was decreased in FLAG immunoprecipitates after overexpression of ALAE in HEK293 cells expressing KH1-4-GFP-FLAG. n = 3. \*\*\*p < 0.001 versus vector.

(B) qPCR analysis and representative immunoblots showed that association of endogenous *Gap43* mRNA with KHSRP was increased in the KHSRP immunoprecipitates after knockdown of ALAE in PC12 cells. n = 3. \*p < 0.05 versus siNC.

(C) qPCR analysis and representative immunoblots showed that the KH3-4 domains were required for KHSRP interaction with *Gap43-3' UTR* in HEK293 cells. n = 4. \*\*p < 0.01 versus KH1-4-GFP-FLAG.

(D) Representative images (left) and quantitative data (right) showed that knockdown of ALAE in the axon compartment significantly increased the percentage of axonal co-localization of KHSRP and *Gap43* mRNA. siNC, n = 23; siALAE, n = 19. \*p < 0.05 versus siNC. Scale bar, 10  $\mu\text{m}$ .

(E) A proposed model for the decoy effect of ALAE by impeding the interaction with KHSRP on *Gap43* mRNA.

(F) Representative images (left) and quantitative data (right) showed that the reduced newly synthesized GAP43 in axons because of siALAE in the cell body compartment was largely rescued by knockdown of KHSRP. GFP was used to indicate the axon profile. siNC, n = 28; siALAE, n = 35; siALAE+ siKHSRP, n = 28. \*\*\*p < 0.001 versus siNC and ###p < 0.001 versus indicated. Scale bar, 10  $\mu\text{m}$ .

(legend continued on next page)

Immunoblotting showed that the reduced level of GAP43 after knockdown of *ALAE* in cultured P0 DRG neurons was rescued fully by coexpression of the *ALAE* 318–351 sense fragment (Figure S7A), suggesting that *ALAE* 318–351 is sufficient for the effect of *ALAE* on GAP43 expression. To determine the role of *ALAE* in KHSRP-mediated translational repression on *Gap43* mRNA, we designed a locked nucleic acid (LNA)-modified antisense to *ALAE* 318–351 to specifically impair the interaction of *ALAE* with KHSRP (Figure 7A). As a control, an LNA-modified scramble was used. To evaluate the competitive effect of *ALAE* 318–351 antisense, we performed RIP experiments in cultured P0 DRG neurons (Figure 7B). qPCR showed that, compared with the control, the amount of *ALAE* co-immunoprecipitated by the KHSRP antibody was decreased significantly, and the amount of *Gap43* mRNA bound to KHSRP was increased in DRG neurons transfected with 50 nM *ALAE* 318–351 antisense (Figures 7C and S7B), indicating that the KHSRP released from *ALAE* association recruits more *Gap43* mRNA. Importantly, application of *ALAE* 318–351 antisense in the axon compartment significantly decreased the protein level of GAP43 in axons but not cell bodies (Figure 7D). The amount of the calmodulin control was not affected in cell bodies or axons (Figure 7D). Transfection with *ALAE* 318–351 antisense in the axon compartment did not affect the level of *ALAE* or the *Gap43* and *Calm1* mRNAs (Figure 7E). Moreover, application of *ALAE* 318–351 antisense significantly reduced newly synthesized GAP43 protein in axons (Figure 7F), suggesting that disruption of the interaction between *ALAE* and KHSRP inhibits local translation of *Gap43* mRNA. Obviously, application of *ALAE* 318–351 antisense in the axon compartment reduced axon elongation rate (Figure 7G). These data suggest that *ALAE* promotes axon elongation by locally preventing KHSRP from binding and inhibiting *Gap43* mRNA translation.

## DISCUSSION

Noncoding RNAs have been suggested to have pivotal roles in axon development by precisely regulating spatiotemporal mRNA translation (Wang and Bao, 2017). In the present study, we propose a working model for the regulatory role of *ALAE* in the process of axon elongation. Under normal conditions, axon-enriched *ALAE* is strongly associated with KHSRP through its ARE for preventing KHSRP binding on *Gap43* mRNA, maintaining GAP43 synthesis and facilitating axon elongation. When *ALAE* is downregulated, a large amount of KHSRP is released, binds *Gap43* mRNA, and represses its translation in the axon, re-

sulting in decreased levels of GAP43 and subsequent slowdown of axon elongation (Figure 7H). Our finding will expand the knowledge of the regulatory roles of axon-enriched lncRNAs during axon development.

### ***ALAE* is a highly axon-enriched and abundant lincRNA required for axon elongation in DRG neurons**

Growing evidence reveals that many molecules are targeted to the axon to regulate the local RNA transcriptome (Cioni et al., 2018). Although the vast majority of miRNAs are localized in the axon and modulate axon development and survival (Hancock et al., 2014; Wang and Bao, 2017), no direct evidence has been reported of the functions and related mechanisms of axon-localized lncRNAs. To determine the existence of axon-localized lncRNAs, we established the lncRNA profile of P0 DRG neurons by RNA-seq combined with bioinformatics analysis and found 462 highly expressed lncRNAs (FPKM > 1). In microfluidic-cultured P0 DRG neurons, *ALAE* was identified as the most enriched and abundant lncRNA in the axon among the top 20 abundant lncRNAs. The abundance of *ALAE* in axons was equivalent to that of *Gap43* and *Calm1*, known as axon-abundant and growth-related mRNAs (Wang et al., 2015; Yu et al., 2018). Moreover, *ALAE* enrichment in axons versus cell bodies is even higher than that of the *Gap43* and *Calm1* mRNAs, strongly supporting a potential role in regulating axon function. Although the axon enrichment and abundance of the top 20 lncRNAs were detected in DRG neurons, other highly expressed lncRNAs have still not been examined extensively because of limited axonal samples and detection methods. Transcriptomics analyses of axon-localized lncRNAs by high-throughput RNA-seq at low-level RNAs needs to be carried out in future studies.

As a highly abundant and enriched axonal lncRNA, *ALAE* was picked up to study function during axon development. Selective knockdown of *ALAE* in axons significantly reduced axon elongation. Regarding the high abundance of *ALAE* in axons, it would be interesting to compare the effects of bulk knockdown in the cell body and exclusive knockdown in the axon. Importantly, our result suggests an equivalent effect by knockdown of *ALAE* in the cell body and axon, emphasizing the crucial contribution of local *ALAE* during axon development. Other lncRNAs, such as *MSTRG.10037* and *MSTRG.15654*, also displayed high abundance and enrichment in axons, implying potential roles of those axon-localized lncRNAs during axon development.

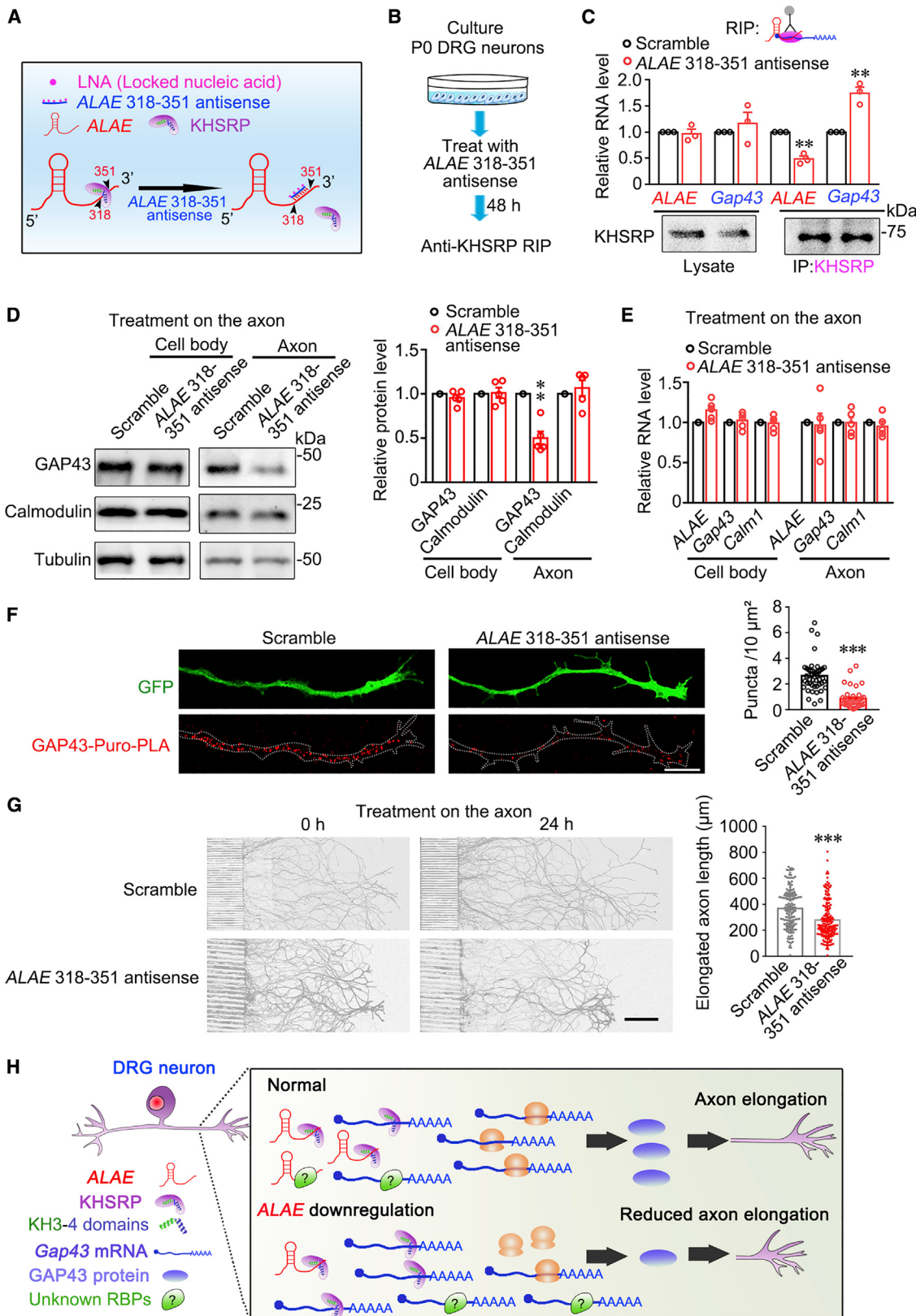
(G) Representative images (left) and quantitative data (right) showed that the reduced axon elongation caused by si*ALAE* in the cell-body compartment was rescued completely by knockdown of KHSRP. siNC, n = 444; si*ALAE*, n = 459; si*ALAE* + siKHSRP, n = 367. \*\*\*p < 0.001 versus siNC and #####p < 0.001 versus indicated. Scale bar, 300 μm.

(H) Representative images (left) and quantitative data (right) showed that the reduced newly synthesized GAP43 in axons because of overexpression of KHSRP in the cell body compartment was rescued completely by coexpression of *ALAE*. GFP was used to indicate the axon profile. Vector, n = 35; KHSRP, n = 35; KHSRP + *ALAE*, n = 28. \*\*\*p < 0.001 versus Vector and #####p < 0.001 versus indicated. Scale bar, 10 μm.

(I) Representative images (left) and quantitative data (right) showed that the reduced axon elongation caused by overexpression of KHSRP in the cell body compartment was completely rescued by coexpression of *ALAE*. Vector, n = 378; KHSRP, n = 322; KHSRP + *ALAE*, n = 290. \*\*\*p < 0.001 versus siNC and #####p < 0.001 versus indicated. Scale bar, 300 μm.

The results are presented as mean ± SEM.

See also Figure S6.



(legend on next page)

### ALAE acts as an RNA decoy to prevent binding and translational repression of KHSRP on Gap43 mRNA during axon elongation

RBPs regulate RNA stability and subcellular targeting in the axons of neurons (Hörnberg and Holt, 2013). KHSRP has been reported to specifically interact and promote the turnover of ARE-containing RNAs (Chen et al., 2001; Gherzi et al., 2004; Giovarelli et al., 2014; Rossi et al., 2019), especially for *Gap43* mRNA in cultured E17.5 hippocampal neurons (Bird et al., 2013). However, the present study showed that KHSRP did not affect the turnover of *Gap43* mRNA in cultured P0 DRG neurons. Hippocampal neurons are highly polarized neurons containing several dendrites and one axon, whereas DRG neurons are pseudo-unipolar neurons with axons only. Interestingly, KHSRP has been reported to control *Tnf* mRNA decay in HeLa cells and regulate *Tnf* mRNA translation in astrocytes (Briata et al., 2016), implicating a cell-dependent effect of KHSRP. Additionally, distinct extrinsic signals from hippocampal and DRG neurons may also specifically activate RBP to differentially regulate its targets. In the present study, we detected that KHSRP interacted with *Gap43* mRNA and repressed its translation. A previous study also showed that KHSRP regulated internal ribosome entry sites (IRES)-dependent translation by stress or viral factors (Kung et al., 2017). More studies are needed to investigate the mechanism of KHSRP controlling mRNA translation in different cell types.

lncRNAs have been shown to recruit interaction partners, especially for RBPs, to regulate gene expression (Guo et al., 2018; Rossi et al., 2019; Yao et al., 2019). In the present study, ALAE was found to bind with the KH3–4 domains of KHSRP via AREs but not other ARE-associated RBPs, such as HuD, suggesting sequence selectivity of the KH domain in KHSRP (Gherzi et al., 2010). The lncRNA H19 has been shown to directly bind the KH1 domain of KHSRP and facilitate degradation of *Myogenin* mRNA during myogenic differentiation (Giovarelli et al., 2014), further highlighting distinct lncRNA-mediated KHSRP functions through specific RNA-binding domains. Notably, we found that the AREs of ALAE and *Gap43* mRNA interacted with the same RNA-binding domain of KHSRP, enabling a competitive role of ALAE over KHSRP binding on *Gap43* mRNA. We speculated that ALAE had strong affinity to bind the KH3–4 domains of KHSRP, releasing KHSRP from the translational repression complex of *Gap43* mRNA. Therefore,

ALAE functions as a molecular decoy to prevent KHSRP-mediated translational repression on *Gap43* mRNA. Previous studies revealed that the lncRNA NORAD, containing multiple PUMILIO (PUM) response elements (PREs), also acts as a decoy to prevent PUM1/PUM2-mediated degradation of a subset of mRNAs with PREs in the cell cycle (Lee et al., 2016; Tichon et al., 2016). These studies suggest a function of lncRNA as a decoy to regulate mRNA translation and degradation in cells.

The association of RBP and its targets is highly dynamic in different types of cells, especially for mRNAs in growing axons, which are rapidly translated in response to extrinsic signaling (Holt and Schuman, 2013). Assembly and disassembly of RBP-RNA granules are also fast and dynamic upon translational regulation (Guo and Shorter, 2015). The low percentage of ALAE co-localization with KHSRP granules detected in the present study also provides evidences to support the dynamic process between RBP and RNA. It is also possible that the interaction of KHSRP with ALAE largely happens outside of granules, according to the highly efficient binding of KHSRP with ALAE detected by RIP. Additionally, although smFISH is a very sensitive method to visualize RNAs, it is still difficult to fully detect ALAE in neurons. Importantly, given the relatively low co-localization of ALAE and KHSRP, ALAE may interact with other RBPs and function as a decoy to regulate the *Gap43* mRNA translation, and those RBPs remain to be identified. Additionally, RBPs have been implicated in directing axonal localization of mRNAs and small noncoding RNAs in our previous study (Wang et al., 2015) and other work (Hörnberg and Holt, 2013). Whether KHSRP interacts with ALAE and mediates axonal targeting of ALAE requires further investigation.

GAP43 is a well-known neuron-specific protein mainly localized in the growth cone of neurons (Verge et al., 1990). The protein level of GAP43 is highly correlated with axon development and regeneration. Regulation of GAP43 synthesis in developing and regenerated axons has been studied extensively (Donnelly et al., 2013). A recent study showed that the lncRNA *slic1* maintained axon regeneration by promoting transcription of the *Sox1* and *Gap43* mRNAs (Perry et al., 2018). Cytoplasm-localized ALAE post-transcriptionally regulated translation of *Gap43* mRNA in the present study, whereas nucleus-localized *slic1* facilitates *Gap43* mRNA directly through transcription activation (Perry et al., 2018), indicating that subcellular distribution of

**Figure 7. Disruption of the interaction between ALAE and KHSRP inhibits translation of *Gap43* mRNA and axon elongation**

- (A) Schematic showing that the interaction between ALAE and KHSRP was reduced by LNA-modified ALAE 318–351 antisense in cultured P0 DRG neurons.
  - (B) Flowchart of RIP for evaluating the competitive effect of ALAE 318–351 antisense on association of ALAE with KHSRP in cultured P0 DRG neurons.
  - (C) qPCR analysis and representative immunoblots showed that association of ALAE with KHSRP was decreased, whereas *Gap43* mRNA was increased in KHSRP immunoprecipitates after application of ALAE 318–351 antisense in cultured P0 DRG neurons. n = 3. \*\*p < 0.01 versus scramble.
  - (D) Representative immunoblots (left) and quantitative data (right) showed that the protein level of GAP43 was decreased by axonal treatment of ALAE 318–351 antisense in microfluidic-cultured P0 DRG neurons. Calmodulin was used as a control that was not affected by treatment. n = 4. \*\*p < 0.01 versus scramble.
  - (E) qPCR analysis showed that the levels of ALAE and *Gap43* mRNA in cell bodies and axons were not affected after axonal application of ALAE 318–351 antisense in microfluidic-cultured P0 DRG neurons. *Calm1* was used as a control that was not affected by treatment. n = 4.
  - (F) Representative images (left) and quantitative data (right) showed that application of ALAE 318–351 antisense significantly reduced newly synthesized GAP43 in the axons of cultured P0 DRG neurons. GFP was used to indicate the axon profile. Scramble, n = 43; ALAE 318–351 antisense, n = 37. \*\*\*p < 0.001 versus scramble. Scale bar, 10 μm.
  - (G) Representative images (left) and quantitative data (right) showed that application of ALAE 318–351 antisense in the axon compartment decreased axon elongation in cultured P0 DRG neurons. Scramble, n = 203; ALAE 318–351 antisense, n = 179. \*\*\*p < 0.001 versus scramble.
  - (H) A proposed model for ALAE required for axon elongation by regulating the repression of KHSRP on *Gap43* mRNA translation.
- The results are presented as mean ± SEM.  
 See also Figure S7.

lincRNAs exerts distinct mechanisms during axon development and regeneration.

Specific blocking of the interplay between lincRNA and RBP is important to evaluate the endogenous effects of lincRNA. Blocking PUM2 binding on mRNAs containing pumilio binding elements (PBEs) using LNA-modified antisense resulted in mislocalization and defective local translation of axonal mRNAs (Martinez et al., 2019), implying efficiency of this method to disrupt the interaction between RNA and RBP. We also utilized a LNA-modified antisense to specifically bind the AREs of *ALAE* and release KHSRP. qPCR detected that the association of *ALAE* with KHSRP was blocked significantly and that the amount of *Gap43* mRNA binding with KHSRP was increased in axons, resulting in decreased local translation of *Gap43* mRNA and subsequent reduction of axon elongation. The present study further explains sequence-based control of the axonal translatome by distinct RBPs.

We identified an axon-enriched lincRNA, *ALAE*, acting as a decoy to interact with KHSRP and prevent its translational suppression on *Gap43* mRNA during axon development. These results reveal a regulatory mechanism for lincRNA involved in spatiotemporal control of local translation in the axon.

## STAR★METHODS

Detailed methods are provided in the online version of this paper and include the following:

- KEY RESOURCE TABLE

- RESOURCE AVAILABILITY

- Lead contact
- Materials availability
- Data and code availability

- EXPERIMENTAL MODEL AND SUBJECT DETAILS

- Animals
- Cell lines
- Primary culture of DRG neurons

- METHOD DETAILS

- Plasmids
- Rapid amplification of cDNA end (RACE)
- Cell transfection and AAV infection
- siRNA and *ALAE*-related fragments
- Immunostaining
- Immunoblotting
- RNA extraction, RT-PCR and quantitative PCR
- Single molecule in situ hybridization
- Detection of axon elongation
- RNA pull-down and mass spectrometry
- RNA immunoprecipitation (RIP)
- RNA stability detection
- Puromycylation-PLA assay

- QUANTIFICATION AND STATISTICAL ANALYSIS

- RNA-seq analysis and lincRNA profiling
- Statistical analysis

## SUPPLEMENTAL INFORMATION

Supplemental information can be found online at <https://doi.org/10.1016/j.celrep.2021.109053>.

## ACKNOWLEDGMENTS

We thank Kai Hao and Dr. Xueliang Zhu for assistance with the puro-PLA method. We also thank Dr. Chao Peng and Yue Yin of the Mass Spectrometry System at the National Facility for Protein Science in Shanghai (NFPS), Zhangjiang Lab, Shanghai Advanced Research Institute, Chinese Academy of Sciences, China for data collection and analyses. This work was supported by grants from the National Natural Science Foundation of China (31671058 and 32070967), the Strategic Priority Research Program of the Chinese Academy of Sciences (XDB19000000), the Shanghai Science and Technology Committee (18JC1420301), and the Youth Innovation Promotion Association of the Chinese Academy of Sciences (Y719S41571).

## AUTHOR CONTRIBUTIONS

M.W. performed the majority of experiments and analyzed data. J.H. detected axon elongation and helped with immunoblotting with B.J. G.-W.L. analyzed RNA-seq data and was supervised by L.Y. X.L. made microfluidic devices and was instructed by X.J. B.W., L.B., and M.W. designed the research and wrote the manuscript. X.Z. and H.C. provided instruction for some experiments.

## DECLARATION OF INTERESTS

The authors declare no competing interests.

Received: June 16, 2020

Revised: October 5, 2020

Accepted: April 7, 2021

Published: May 4, 2021

## REFERENCES

- Bird, C.W., Gardiner, A.S., Bolognani, F., Tanner, D.C., Chen, C.Y., Lin, W.J., Yoo, S., Twiss, J.L., and Perrone-Bizzozero, N. (2013). KSRP modulation of GAP-43 mRNA stability restricts axonal outgrowth in embryonic hippocampal neurons. *PLoS ONE* 8, e79255.
- Briata, P., Bordo, D., Puppo, M., Gorlero, F., Rossi, M., Perrone-Bizzozero, N., and Gherzi, R. (2016). Diverse roles of the nucleic acid-binding protein KHSRP in cell differentiation and disease. *Wiley Interdiscip. Rev. RNA* 7, 227–240.
- Briese, M., Saal, L., Appenzeller, S., Moradi, M., Baluapuri, A., and Sendtner, M. (2016). Whole transcriptome profiling reveals the RNA content of motor axons. *Nucleic Acids Res.* 44, e33.
- Briggs, J.A., Wolvetang, E.J., Mattick, J.S., Rinn, J.L., and Barry, G. (2015). Mechanisms of Long Non-coding RNAs in Mammalian Nervous System Development, Plasticity, Disease, and Evolution. *Neuron* 88, 861–877.
- Cabili, M.N., Trapnell, C., Goff, L., Koziol, M., Tazon-Vega, B., Regev, A., and Rinn, J.L. (2011). Integrative annotation of human large intergenic noncoding RNAs reveals global properties and specific subclasses. *Genes Dev.* 25, 1915–1927.
- Carlevaro-Fita, J., and Johnson, R. (2019). Global positioning system: understanding long noncoding RNAs through subcellular localization. *Mol. Cell* 73, 869–883.
- Chen, C.Y., Gherzi, R., Ong, S.E., Chan, E.L., Rajmakers, R., Pruijn, G.J., Stoecklin, G., Moroni, C., Mann, M., and Karin, M. (2001). AU binding proteins recruit the exosome to degrade ARE-containing mRNAs. *Cell* 107, 451–464.
- Chen, X.Q., Wang, B., Wu, C., Pan, J., Yuan, B., Su, Y.Y., Jiang, X.Y., Zhang, X., and Bao, L. (2012). Endosome-mediated retrograde axonal transport of P2X3 receptor signals in primary sensory neurons. *Cell Res.* 22, 677–696.
- Cioni, J.M., Koppers, M., and Holt, C.E. (2018). Molecular control of local translation in axon development and maintenance. *Curr. Opin. Neurobiol.* 51, 86–94.
- Dajas-Bailador, F., Bonev, B., Garcez, P., Stanley, P., Guillermot, F., and Papalopulu, N. (2012). microRNA-9 regulates axon extension and branching by targeting Map1b in mouse cortical neurons. *Nat. Neurosci.* 15, 697–699.
- Donnelly, C.J., Park, M., Spillane, M., Yoo, S., Pacheco, A., Gomes, C., Vuppalanchi, D., McDonald, M., Kim, H.H., Merienda, T.T., et al. (2013). Axonally

- synthesized β-actin and GAP-43 proteins support distinct modes of axonal growth. *J. Neurosci.* 33, 3311–3322.
- Eddy, S.R. (2011). Accelerated Profile HMM Searches. *PLoS Comput. Biol.* 7, e1002195.
- El-Gebali, S., Mistry, J., Bateman, A., Eddy, S.R., Luciani, A., Potter, S.C., Qureshi, M., Richardson, L.J., Salazar, G.A., Smart, A., et al. (2019). The Pfam protein families database in 2019. *Nucleic Acids Res.* 47 (D1), D427–D432.
- Gherzi, R., Lee, K.Y., Briata, P., Wegmüller, D., Moroni, C., Karin, M., and Chen, C.Y. (2004). A KH domain RNA binding protein, KSRP, promotes ARE-directed mRNA turnover by recruiting the degradation machinery. *Mol. Cell* 14, 571–583.
- Gherzi, R., Chen, C.Y., Trabucchi, M., Ramos, A., and Briata, P. (2010). The role of KSRP in mRNA decay and microRNA precursor maturation. *Wiley Interdiscip. Rev. RNA* 1, 230–239.
- Giovarelli, M., Bucci, G., Ramos, A., Bordo, D., Wilusz, C.J., Chen, C.Y., Puppo, M., Briata, P., and Gherzi, R. (2014). H19 long noncoding RNA controls the mRNA decay promoting function of KSRP. *Proc. Natl. Acad. Sci. USA* 111, E5023–E5028.
- Gumy, L.F., Yeo, G.S., Tung, Y.C., Zivraj, K.H., Willis, D., Coppola, G., Lam, B.Y., Twiss, J.L., Holt, C.E., and Fawcett, J.W. (2011). Transcriptome analysis of embryonic and adult sensory axons reveals changes in mRNA repertoire localization. *RNA* 17, 85–98.
- Guo, L., and Shorter, J. (2015). It's raining liquids: RNA tunes viscoelasticity and dynamics of membraneless organelles. *Mol. Cell* 60, 189–192.
- Guo, Y., Chen, X., Xing, R., Wang, M., Zhu, X., and Guo, W. (2018). Interplay between FMRP and lncRNA TUG1 regulates axonal development through mediating SnoN-Ccd1 pathway. *Hum. Mol. Genet.* 27, 475–485.
- Hancock, M.L., Preitner, N., Quan, J., and Flanagan, J.G. (2014). MicroRNA-132 is enriched in developing axons, locally regulates Rasa1 mRNA, and promotes axon extension. *J. Neurosci.* 34, 66–78.
- Hao, S., and Baltimore, D. (2009). The stability of mRNA influences the temporal order of the induction of genes encoding inflammatory molecules. *Nat. Immunol.* 10, 281–288.
- Holt, C.E., and Schuman, E.M. (2013). The central dogma decentralized: new perspectives on RNA function and local translation in neurons. *Neuron* 80, 648–657.
- Hörnberg, H., and Holt, C. (2013). RNA-binding proteins and translational regulation in axons and growth cones. *Front. Neurosci.* 7, 81.
- Hwang, I., Cao, D., Na, Y., Kim, D.Y., Zhang, T., Yao, J., Oh, H., Hu, J., Zheng, H., Yao, Y., and Paik, J. (2018). Far upstream element-binding protein 1 regulates LSD1 alternative splicing to promote terminal differentiation of neural progenitors. *Stem Cell Reports* 10, 1208–1221.
- Kang, Y.J., Yang, D.C., Kong, L., Hou, M., Meng, Y.Q., Wei, L., and Gao, G. (2017). CPC2: a fast and accurate coding potential calculator based on sequence intrinsic features. *Nucleic Acids Res.* 45 (W1), W12–W16.
- Kar, A.N., Lee, S.J., and Twiss, J.L. (2018). Expanding axonal transcriptome brings new functions for axonally synthesized proteins in health and disease. *Neuroscientist* 24, 111–129.
- Kim, D., Langmead, B., and Salzberg, S.L. (2015). HISAT: a fast spliced aligner with low memory requirements. *Nat. Methods* 12, 357–360.
- Kung, Y.A., Hung, C.T., Chien, K.Y., and Shih, S.R. (2017). Control of the negative IRES trans-acting factor KHSRP by ubiquitination. *Nucleic Acids Res.* 45, 271–287.
- Lee, S., Kopp, F., Chang, T.C., Sataluri, A., Chen, B., Sivakumar, S., Yu, H., Xie, Y., and Mendell, J.T. (2016). Noncoding RNA NORAD regulates genomic stability by sequestering PUMILIO proteins. *Cell* 164, 69–80.
- Liao, Y., Smyth, G.K., and Shi, W. (2014). featureCounts: an efficient general purpose program for assigning sequence reads to genomic features. *Bioinformatics* 30, 923–930.
- Lin, N., Chang, K.Y., Li, Z., Gates, K., Rana, Z.A., Dang, J., Zhang, D., Han, T., Yang, C.S., Cunningham, T.J., et al. (2014). An evolutionarily conserved long noncoding RNA TUNA controls pluripotency and neural lineage commitment. *Mol. Cell* 53, 1005–1019.
- Martinez, J.C., Randolph, L.K., Iascone, D.M., Pernice, H.F., Polleux, F., and Hengst, U. (2019). Pum2 Shapes the Transcriptome in Developing Axons through Retention of Target mRNAs in the Cell Body. *Neuron* 104, 931–946.e5.
- Mueller, F., Senecal, A., Tantale, K., Marie-Nelly, H., Ly, N., Collin, O., Basuyk, E., Bertrand, E., Darzacq, X., and Zimmer, C. (2013). FISH-quant: automatic counting of transcripts in 3D FISH images. *Nat. Methods* 10, 277–278.
- Perry, R.B., Hezroni, H., Goldrich, M.J., and Ulitsky, I. (2018). Regulation of neuroregeneration by long noncoding RNAs. *Mol. Cell* 72, 553–567.e5.
- Pertea, M., Pertea, G.M., Antonescu, C.M., Chang, T.C., Mendell, J.T., and Salzberg, S.L. (2015). StringTie enables improved reconstruction of a transcriptome from RNA-seq reads. *Nat. Biotechnol.* 33, 290–295.
- Ramos, A.D., Andersen, R.E., Liu, S.J., Nowakowski, T.J., Hong, S.J., Gertz, C., Salinas, R.D., Zarabi, H., Kriegstein, A.R., and Lim, D.A. (2015). The long noncoding RNA Pnky regulates neuronal differentiation of embryonic and postnatal neural stem cells. *Cell Stem Cell* 16, 439–447.
- Ransohoff, J.D., Wei, Y., and Khavari, P.A. (2018). The functions and unique features of long intergenic non-coding RNA. *Nat. Rev. Mol. Cell Biol.* 19, 143–157.
- Rossi, M., Bucci, G., Rizzotto, D., Bordo, D., Marzi, M.J., Puppo, M., Flinois, A., Spadaro, D., Citi, S., Emionite, L., et al. (2019). LncRNA EPR controls epithelial proliferation by coordinating Cdkn1a transcription and mRNA decay response to TGF-β. *Nat. Commun.* 10, 1969.
- Shigeoka, T., Jung, H., Jung, J., Turner-Bridger, B., Ohk, J., Lin, J.Q., Amieux, P.S., and Holt, C.E. (2016). Dynamic axonal translation in developing and mature visual circuits. *Cell* 166, 181–192.
- Tichon, A., Gil, N., Lubelsky, Y., Havkin Solomon, T., Lemze, D., Itzkovitz, S., Stern-Ginossar, N., and Ulitsky, I. (2016). A conserved abundant cytoplasmic long noncoding RNA modulates repression by Pumilio proteins in human cells. *Nat. Commun.* 7, 12209.
- tom Dieck, S., Kochen, L., Hanus, C., Heumüller, M., Bartrik, I., Nassim-Assir, B., Merk, K., Mosler, T., Garg, S., Bunse, S., et al. (2015). Direct visualization of newly synthesized target proteins in situ. *Nat. Methods* 12, 411–414.
- Tsanov, N., Samacoits, A., Chouaib, R., Traboulsi, A.M., Gostan, T., Weber, C., Zimmer, C., Zibara, K., Walter, T., Peter, M., et al. (2016). smiFISH and FISH-quant - a flexible single RNA detection approach with super-resolution capability. *Nucleic Acids Res.* 44, e165.
- Verge, V.M., Tetzlaff, W., Richardson, P.M., and Bisby, M.A. (1990). Correlation between GAP43 and nerve growth factor receptors in rat sensory neurons. *J. Neurosci.* 10, 926–934.
- Wang, B., and Bao, L. (2017). Axonal microRNAs: localization, function and regulatory mechanism during axon development. *J. Mol. Cell Biol.* 9, 82–90.
- Wang, C., and Fang, J. (2015). RLM-RACE, PPM-RACE, and qRT-PCR: an integrated strategy to accurately validate miRNA target genes. *Methods Mol. Biol.* 1296, 175–186.
- Wang, L., Park, H.J., Dasari, S., Wang, S., Kocher, J.P., and Li, W. (2013). CPAT: Coding-Potential Assessment Tool using an alignment-free logistic regression model. *Nucleic Acids Res.* 41, e74.
- Wang, B., Pan, L., Wei, M., Wang, Q., Liu, W.W., Wang, N., Jiang, X.Y., Zhang, X., and Bao, L. (2015). FMRP-mediated axonal delivery of miR-181d regulates axon elongation by locally targeting Map1b and Calm1. *Cell Rep.* 13, 2794–2807.
- Yao, R.W., Wang, Y., and Chen, L.L. (2019). Cellular functions of long noncoding RNAs. *Nat. Cell Biol.* 21, 542–551.
- Yoo, S., Kim, H.H., Kim, P., Donnelly, C.J., Kalinski, A.L., Vuppala, D., Park, M., Lee, S.J., Merlano, T.T., Perrone-Bizzozero, N.I., and Twiss, J.L. (2013). A HuD-ZBP1 ribonucleoprotein complex localizes GAP-43 mRNA into axons through its 3' untranslated region AU-rich regulatory element. *J. Neurochem.* 126, 792–804.
- Yu, J., Chen, M., Huang, H., Zhu, J., Song, H., Zhu, J., Park, J., and Ji, S.J. (2018). Dynamic m6A modification regulates local translation of mRNA in axons. *Nucleic Acids Res.* 46, 1412–1423.

## STAR★METHODS

## KEY RESOURCE TABLE

REAGENT or RESOURCE	SOURCE	IDENTIFIER
<b>Antibodies</b>		
Rabbit monoclonal anti-KHSRP	Abcam	Cat#: ab150393; RRID: N/A
Rabbit monoclonal anti-FUBP1	Abcam	Cat#: ab181111; RRID: N/A
Rabbit polyclonal anti-GAP43	Chemicon	Cat#: AB5220; RRID: AB_2107282
Mouse monoclonal anti-tubulin	Sigma-Aldrich	Cat#: T5168; RRID: AB_477579
Mouse monoclonal anti-Tau-1	Chemicon	Cat#: MAB3420; RRID: AB_94855
Chicken polyclonal anti-beta III Tubulin	Abcam	Cat#: ab107216; RRID: AB_10899689
Mouse monoclonal anti-HuR	Santa Cruz	Cat#: sc-5261; RRID: AB_627770
Mouse monoclonal anti-HuD	Santa Cruz	Cat#: sc-28299; RRID: AB_627765
Mouse monoclonal anti-Lamin B1	Proteintech	Cat#: 66095-1-Ig; RRID: AB_11232208
Mouse monoclonal anti-calmodulin	Millipore	Cat#: 05-173; RRID: AB_309644
Mouse monoclonal anti-GAPDH	Abcam	Cat#: ab8245; RRID: AB_2107448
Mouse monoclonal anti-FLAG	Origene	Cat#: TA50011-100; RRID: AB_2622345
Mouse monoclonal anti-puromycin	Millipore	Cat# MABE343; RRID: AB_2566826
Goat anti-Mouse IgG HRP conjugate	Chemicon	Cat#: 24031340; RRID: N/A
Goat anti-Rabbit IgG HRP conjugate	Chemicon	Cat#: 24070101; RRID: N/A
Goat anti-Rabbit Secondary Antibody, Alexa Fluor 488	Invitrogen	Cat#: A-11034; RRID: AB_2576217
Goat anti-Mouse Secondary Antibody, Alexa Fluor 488	Invitrogen	Cat# A-21042; RRID: AB_2535711
Goat anti-Rabbit Secondary Antibody, Alexa Fluor 555	Invitrogen	Cat# A-21430; RRID: AB_2535851
Goat anti-Chicken Secondary Antibody, Alexa Fluor 647	Invitrogen	Cat# A-21449; RRID: AB_2535866
<b>Chemicals, peptides, and recombinant proteins</b>		
Ribonucleoside Vanadyl Complex	NEB	Cat#: S1420S
cComplete ULTRA Tablets, Mini, EASYPack Protease Inhibitor Cocktail	Roche	Cat#: 5892970001
Lipofectamine 2000 Transfection Reagent	Invitrogen	Cat#: 11668019
Lipofectamine RNAiMAX Transfection Reagent	Invitrogen	Cat#: 13778150
DAPI	Invitrogen	Cat#: D1306
Triton X-100	Sangon Biotech	Cat#: A110694
NP40	Sangon Biotech	Cat#: A100777
Bovine Serum Albumin	ABCone	Cat#: B24726
Actinomycin D	MedChemExpress	Cat#: HY-17559
Puromycin	Sigma-Aldrich	Cat#: p8833
Paraformaldehyde	Sinopharm Chemical Reagent Co., Ltd	Cat#: 80096618
<b>Critical commercial assays</b>		
Hieff Clone One Step Cloning Kit	Yeasen	Cat#: 10911ES25
KOD-Plus-Neo kit	Toyobo	Cat#: F1066K
SuperScript III Reverse Transcriptase	Invitrogen	Cat#: 18080044
PrimeScript RT reagent Kit (Perfect Real Time)	Takara	Cat#: RR037A

(Continued on next page)

**Continued**

REAGENT or RESOURCE	SOURCE	IDENTIFIER
Hieff® qPCR SYBR Green Master Mix (Low Rox Plus)	Yeasen	Cat#: 11202ES03
Pierce RNA 3' End Desthiobiotinylation Kit	Thermo scientific	Cat#: 20163
Pierce Magnetic RNA-Protein Pull-Down Kit	Thermo scientific	Cat#: 20164
Alexa Fluor 555 Tyramide SuperBoost Kit, goat anti-mouse IgG	Invitrogen	Cat#: B40913
Duolink™ <i>In Situ</i> detection Regents Red	Sigma-Aldrich	Cat#: DUO92008
Duolink <i>In Situ</i> PLA® Probe Anti-Rabbit PLUS	Sigma-Aldrich	Cat#: DUO92002
Duolink <i>In Situ</i> PLA® Probe Anti-Mouse MINUS	Sigma-Aldrich	Cat#: DUO92004
Duolink <i>In Situ</i> Wash Buffers, Fluorescence	Sigma-Aldrich	Cat#: DUO82049
<b>Deposited data</b>		
RNA-seq raw files	This paper	GEO: GSE151615
Mass spectrometry raw files	This paper	PX: PXD019429
<b>Experimental models: cell lines</b>		
HEK293	Cell bank of Chinese Academy of Sciences	Cat#: GNHu18
PC12	Cell bank of Chinese Academy of Sciences	Cat#: TCR8
<b>Experimental models: Organisms/strains</b>		
Rat: SD	Shang laboratory animal research center, Chinese academy of sciences	N/A
<b>Oligonucleotides</b>		
See <a href="#">Tables S3</a> and <a href="#">S4</a> for DNA and siRNA used in this paper	This paper	N/A
<b>Recombinant DNA</b>		
pcDNA3.1-ALAE	This paper	N/A
pcDNA3.1-ALAE-p223-371	This paper	N/A
pcDNA3.1-ALAE-p223-261	This paper	N/A
pcDNA3.1-ALAE-p262-317	This paper	N/A
pcDNA3.1-ALAE-p318-351	This paper	N/A
pcDNA3.1-ALAE-p352-371	This paper	N/A
pcDNA3.1-ALAE-p1-222	This paper	N/A
pAOV-EGFP-KHSRP-FLAG	This paper	N/A
pAOV-EGFP-KH1-4-FLAG	This paper	N/A
pAOV-EGFP-KH1-4-pKH1-FLAG	This paper	N/A
pAOV-EGFP-KH1-4-pKH2-FLAG	This paper	N/A
pAOV-EGFP-KH1-4-pKH3-FLAG	This paper	N/A
pAOV-EGFP-KH1-4 -pKH4-FLAG	This paper	N/A
pEGFP-GAP43-CDS-3'UTR	This paper	N/A
pcDNA3.1-Gap43 -3' UTR	This paper	N/A
tdTomato-GAP43	This paper	N/A
pEGFP-C3-ALAE	This paper	N/A
pEGFP-N3-ALAE	This paper	N/A
pAKD-CMV-H1-shNC	This paper	N/A
pAKD-CMV-H1-shALAE	This paper	N/A
<b>Software and algorithms</b>		
Fiji/ImageJ	Fiji/ImageJ	<a href="https://imagej.net/Fiji">https://imagej.net/Fiji</a>
Prism	GraphPad Software	<a href="https://www.graphpad.com/">https://www.graphpad.com/</a>

**RESOURCE AVAILABILITY****Lead contact**

Further information and requests for resources and reagents should be directed to and will be fulfilled by the lead contact, Bin Wang ([bin\\_wang2020@163.com](mailto:bin_wang2020@163.com)).

**Materials availability**

Requests for materials generated in this study should be directed to the lead contact, Bin Wang ([bin\\_wang2020@163.com](mailto:bin_wang2020@163.com)), after completing Material Transfer Agreement.

**Data and code availability**

The raw data of RNA-seq has been deposited to Gene Expression Omnibus with the accessed number GSE151615. The raw data of mass spectrometry proteomics has been deposited to ProteomeXchange Consortium with the dataset identifier PXD019429.

**EXPERIMENTAL MODEL AND SUBJECT DETAILS****Animals**

All experiments were approved by the Committee of Use of Laboratory Animals in the Shanghai Institute of Biochemistry and Cell Biology, CAS Center for Excellence in Molecular Cell Science, Chinese Academy of Sciences. The Sprague Dawley (SD) male and female rats at postnatal 0 day (P0) were provided by Shanghai Laboratory Animal Center, Chinese Academy of Sciences.

**Cell lines**

HEK293 cells and PC12 cells were obtained from the Cell bank of Chinese Academy of Sciences. HEK293 cells were cultured in DMEM supplemented with 10% fetal bovine serum (GIBCO) and penicillin/streptomycin. PC12 cells were cultured in RPMI medium 1640 (Invitrogen) containing 15% horse serum and 2.5% fetal bovine serum.

**Primary culture of DRG neurons**

Primary culture of DRG neurons was performed as described previously with minor modifications ([Wang et al., 2015](#)). Briefly, DRGs were dissociated from rats at P0, followed by digestion with a mixture enzyme of collagenase I, trypsin and DNaseI. After centrifugation with 15% Percoll to remove non-neuronal cells, the DRG neurons were obtained and cultured in the neurobasal medium containing 2% B27 supplement, 2 mM L-glutamine (Invitrogen) and 100 ng/ml nerve growth factor (NGF; Invitrogen), and 10 µM 5-fluoro-2'-deoxyuridine (Sigma) was used to inhibit the proliferation of non-neuronal cells.

For compartmental culture of DRG neurons, the microfluidic chamber was fabricated as previously reported ([Chen et al., 2012](#)). Briefly, utilizing a two-step photolithography process (photoresist SU-8 2007 and SU-8 2100), we fabricated the master with a positive relief of two heights. The microfluidic chamber consisted of cell body and axon compartments through microchannels linking the two compartments. The compartment was 100 µm in height, whereas the microchannels were 3-4 µm in height and were allowed to control axon growth. The master was replicated by curing the PDMS (Sylgard 184, Dow Corning) pre-polymer with a curing agent at a ratio of 10:1. After baking 2 h at 80°C, the PDMS mold was peeled off of the master, and the chamber was obtained by placing the mold on a poly-D-lysine-coated glass coverslip. Then, the dissociated DRG neurons were plated into the cell body compartment. The axons crossed the microchannels and reached the axon compartment within 24 h.

**METHOD DETAILS****Plasmids**

The full length of *ALAE* was amplified from rat cDNA and cloned into pcDNA3.1, and all truncations or deletions of *ALAE* were created using KOD-Plus-Mutagenesis Kit (TOYOBO). The coding sequence of KHSRP was amplified from rat cDNA and cloned into pAOV-CMV-bGlobin-GFP to produce KHSRP-GFP-FLAG. All deletions of KHSRP were produced using KOD-Plus-Mutagenesis Kit. The 3'UTR of *Gap43* mRNA was amplified from rat cDNA and cloned into pcDH-CMV-EF1a-GFP to produce *Gap43*-3'UTR-GFP. The CDS-3'UTR of *Gap43* mRNA was amplified from rat cDNA and cloned into pEGFP-C3 to produce GFP-*Gap43*-3'UTR. *Gap43* CDS was amplified from GFP-*Gap43*-3'UTR into ptdTomato to produce tdTomato-GAP43.

For AAV construction, the shRNA for *ALAE* and the negative control shRNA were cloned into the pAKD-CMV-bGlobin-eGFP-H1-shRNA, respectively. The AAV2-based vector pseudotyped with AAV8 serotype capsid (AAV2/8) was purchased and supplied in titters  $3 \times 10^{12}$  (Obio Technology, China). The sequences of *ALAE*, KHSRP and control shRNA were indicated in [Table S2](#).

**Rapid amplification of cDNA end (RACE)**

The method for obtaining the full length of *ALAE* was adopted from previous study ([Wang and Fang, 2015](#)). The RNA ligase-mediated (RLM)-RACE approach was performed to obtain the unknown 3' and 5' end sequences of *ALAE* by using FirstChoice RLM-RACE Kit (Ambion, Inc.). Briefly, the 3'RACE and 5'RACE cDNA libraries were first established from P0 DRGs. Then, the RLM-RACE PCR was

performed with *ALAE*-specific primers to obtain the product that was further sequenced. Finally, the full-length sequence of *ALAE* was verified by comparing the sequencing result with the predicted sequence.

### Cell transfection and AAV infection

Transfection of plasmids was carried out with lipofectamine 2000 (Invitrogen) according to the manufacturer's protocol. Transient expression with siRNA was performed with RNAiMAX (Invitrogen) according to the manufacturer's protocol. For electroporation of DRG neurons, cells were suspended in electroporation buffer and then electroporated by Nucleofector II (Amaxa) using the program named O-003. AAV infection was performed directly by adding the virus in titers  $3 \times 10^{12}$  to the culture medium at the dilution 1:50.

### siRNA and *ALAE*-related fragments

The siRNA, LNA-modified blocker and *ALAE* sense fragment (Guangzhou RiboBio Co. Ltd., China) were synthesized. Sequences were indicated in [Table S2](#). Scramble and *ALAE* 318–351 antisense were custom-designed for serving as a negative control and disrupting the interaction between KHSRP and *ALAE*, respectively.

To obtain the *ALAE*<sup>R</sup> RNA, double stand DNA of *ALAE*<sup>R</sup> without si*ALAE* targeting region was amplified from pcDNA-*ALAE* attached with T7 sequence in 5' end. After purified by ethanol, *ALAE*<sup>R</sup> RNA was transcribed by using T7 polymerase (Promega). For the rescue experiment of *ALAE*<sup>R</sup>, 10 pg *ALAE*<sup>R</sup> RNA was mixed with the si*ALAE* in Opti-MEM medium. After mixture with RNAiMax (Invitrogen) for 15 min, they were added to the axon compartment of microfluidic-cultured P0 DRG neurons. Further analysis of the RNA or protein was conducted 48 h after transfection.

### Immunostaining

Cells plated on the dish were fixed in 4% paraformaldehyde for 15 min at room temperature. Then, the cells were incubated with the indicated primary antibodies overnight at 4°C followed by secondary antibodies conjugated with fluorescent dye (1:1000; Jackson Immunoresearch) for 45 min at 37°C. Fluorescence images were acquired from Leica SP8 confocal microscopy (Leica).

### Immunoblotting

Tissues, cell lysates or beads were incubated in SDS-PAGE loading buffer for 5 min at 95°C. The samples were separated on SDS-PAGE, transferred, probed with the indicated antibodies, and visualized with enhanced chemiluminescence (Amersham Biosciences). The intensity of immunoreactive bands was analyzed with the Image-Pro Plus 5.1 software (Media Cybernetics).

### RNA extraction, RT-PCR and quantitative PCR

Total RNA was extracted from tissues or cultured cells with TRIzol reagent according to the manufacturer's protocol. To obtain the RNA from the cell bodies and axons, TRIzol reagent was used to dissolve samples in the cell body and axon compartments, respectively. Three microfluidic chambers were collected for the axonal RNA dissolved in 5 µl RNase free water whereas the RNA from cell bodies dissolved in 50 µl RNase free water. The RNA was then treated with gDNA eraser to degrade possible genomic DNA pollution before reverse-transcription with the PrimerScript RT Reagent Kit (TaKaRa). For the reverse transcription, total axonal RNA and 1% cell body RNA were used in cDNA synthesis for qPCR analysis. For qPCR, the cDNA synthesis was carried out with oligo (dT) and random hexamers. For gene amplification, the cDNA was obtained with gene-specific primers. qPCR was performed using HieffTM qPCR SYBR Green Master Mix (Yeasen) and Lightcycler R 96 System (Roche). The qPCR results were analyzed and normalized to *Gapdh* mRNA for the relative mRNA or lincRNA level, which were then convert to the fold change. For the microfluidic-cultured P0 DRG neurons, the relative abundance level for distinct lincRNAs and mRNAs were normalized to *Gapdh* mRNA. The axon enrichment ratio for lincRNAs or mRNAs were calculated by the ratio of abundance level in the axons to the cell bodies. Primer sequences for qPCR were provided in [Table S3](#).

### Single molecule *in situ* hybridization

We performed *in situ* hybridization with SmFISH as previously described ([Tsanov et al., 2016](#)). Primary DNA probes for *ALAE* and *Gap43* mRNA were kindly designed by Dr. Marion Peter (sequences were indicated in [Table S4](#)) and synthesized (Invitrogen), and the secondary probe was tailed with DIG at both ends. Primary probe and second probe were hybridized at sequential temperature with 85°C 3 min, 65°C 3 min and 25°C 5 min in the hybridization buffer (100 mM NaCl, 50 mM Tris-HCl, 10 mM MgCl<sub>2</sub>, pH 7.9). HEK293 cells or cultured DRG neurons were fixed in 4% paraformaldehyde and hybridized with the primary-second probe duplex at 37°C overnight. After washing, cells were incubated with anti-DIG-POD (Roche) and other antibodies for immunostaining at 4°C overnight. The signal was amplified by the TSA™ Plus fluorescein and Cy3 System (PerkinElmer) according to the manufacturer's protocol. If other antibodies for immunostaining were used, the cells need to be further incubated with related secondary antibodies conjugated with fluorescent dye at 37°C for 45 min before TSA amplification. Fluorescent images were acquired from Leica SP8 confocal microscopy. Percentage of co-localized granules was analyzed according to previous report ([Chen et al., 2012](#)). Briefly, the percentage of colocalization was quantified by Image-pro Plus 5.1 software and defined as the overlapping area with a mean diameter > 2 pixels between two granules at least 5 pixels per diameter within individual cell body or axon.

**Detection of axon elongation**

The elongated axon growth was measured as described previously with minor modifications (Wang et al., 2015). In microfluidic-cultured P0 DRG neurons in the presence of 100 ng/ml NGF, the neurons electroporated with GFP to clearly visualize the process of axon elongation were transfected with siRNA, LNAs and RNA fragment in the cell body compartment or axon compartment. The images of axons in the axon compartment were captured by the PerkinElmer UltraView Vox system (PerkinElmer) using a 10 × lens. Then, each photograph was stitched to produce an integrated image for whole axon compartment. After 8 and 24 h, the second image was produced at the same axon compartment. The increase of single axon length clearly detected during 8 and 24 h was analyzed using the plug-in of Simple neurite tracer from ImageJ (NIH). At least 3 chambers and total 100 axons per group in 3 independent experiments were performed for quantitative analysis.

**RNA pull-down and mass spectrometry**

This assay was performed according to the manufacturer's protocol (Thermo Fisher Scientific) with minor modifications. The products of full-length *ALAE* fused with T7 promoter sequence were transcribed using the T7 RNA Polymerase (Promega). Biotin-labeled sense and antisense of *ALAE* were obtained using Pierce™ RNA 3' End Desthiobiotinylation Kit (Thermo Fisher Scientific). Then, 20 pM biotinylated RNA was incubated with 50 µl streptavidin magnetic beads for 30 min in the washing buffer. DRGs or PC12 cells were lysed with Pierce IP lysis buffer (Thermo Fisher Scientific) with RNase inhibitor and protease inhibitor cocktail. After centrifuging at 13,000 g for 10 min at 4°C, the supernatant was collected, 5% of which was saved for immunoblotting as lysate, and the rest was added to the probe-beads and incubated at 4°C overnight. After washing for three times, one fourth of the beads were added to 500 µl TRIzol reagent for RNA extraction. To harvest proteins, the rest beads were eluted with elution buffer (95% formamide with 5% ethylenediaminetetraacetic acid) at 95°C for 5 min. RNA-captured proteins were analyzed by immunoblotting and subjected to mass spectrometry analysis at core facility of molecular biology (Shanghai Institute of Biochemistry and Cell Biology, Chinese Academy of Sciences). The raw data of mass spectrometry proteomics has been deposited to ProteomeXchange Consortium with the dataset identifier PXD019429. The mass spectrometry result from *ALAE* pull-down experiment was provided in Table S2.

**RNA immunoprecipitation (RIP)**

HEK293 cells or DRG tissues were harvested and lysed with RIPA buffer (100 mM KCl, 5 mM MgCl<sub>2</sub>, 10 mM HEPES-NaOH, 0.5% NP-40) with RNase inhibitor (Promega) and protease inhibitor cocktail (Roche). The 50 µl protein G beads (Sigma) were incubated with 1 µg antibody at room temperature for 1 h in the washing buffer (50 mM Tris, pH 7.4; 150 mM NaCl, 1 mM MgCl<sub>2</sub>, 0.05% NP-40). Then, the resulting supernatant was incubated with the antibody conjugated with immobilized beads at 4°C for 3 h. The same amount of IgG was used as a control. The protein-captured beads were washed with the wash buffer for 3 times. RNA extraction and immunoblotting from the beads were further carried out by using TRIzol (Invitrogen) and loading buffer, respectively, for subsequent detection of co-immunoprecipitated RNA and protein.

**RNA stability detection**

Actinomycin D (ActD) was utilized as a transcriptional inhibitor in the detection of RNA stability as previously reported (Hao and Baltimore, 2009). P0 DRG neurons were cultured for 24 h and then transfected with siNC or siKHSRP for 48 h. Then, the neurons were applied with 10 µM ActD (MedChemExpress) for 0, 2, 4 and 6 h, respectively. RNA extraction and immunoblotting from those samples were further carried out by using TRIzol (Invitrogen) and protein loading buffer, respectively, for subsequent detection of RNA and protein. The statistical analysis was conducted using two-way ANOVA to compare the effect of siRNA treatment on the mRNA level at different time points.

**Puromycylation-PLA assay**

The puromycylation-PLA assay was performed according to previous study (tom Dieck et al., 2015) with slight modifications. Briefly, cultured P0 DRG neurons after transfected with siRNA or LNA for 48 h were treated with 100 µg/ml cycloheximide (Sigma) for 30 min at 37°C. Then, the cells were incubated with the medium containing 1 µM puromycin (Sigma) for 10 min at 37°C and fixed with 4% paraformaldehyde for 20 min. The following PLA detection was carried out by Duolink reagents (Sigma) according to the manufacturer's instructions. Detection of newly synthesized GAP43 by proximity ligation was performed by using anti-GAP43 and anti-puromycin. The antibody combination was applied to the cells and incubated at 4°C overnight. Then the cells were incubated with probes including PLA<sup>minus</sup> and PLA<sup>plus</sup> in a 1:5 dilution 1 h and ligated with T4 ligase for 30 min at 37 °C. After ligation, polymerase and fluorophore-labeled detection oligo were added to the cell to initiate and amplify signals for 100 min at 37 °C. Finally, cells were incubated with DAPI and then mounted with a coverslip. Images were acquired with Leica SP8 confocal microscope using a 63 × /1.4-NA oil lens.

Quantification of the PLA punctum per area was performed by Fish Quant v3a according to previous study (Mueller et al., 2013). Raw images imported to Fish Quant were filtered by the Dual-Gaussian filter to define the value of Kernel BGD and Kernel SNR with 0.5 pixel. The axons were drawn manually based on the GFP signals and Puro-PLA signals within the GFP area were automatically detected. Finally, the number of Punctum per selected area was calculated.

## QUANTIFICATION AND STATISTICAL ANALYSIS

### RNA-seq analysis and lincRNA profiling

Total RNAs were extracted from cultured P0 DRG neurons according to the manufacturer's protocol. The RNA-Seq library preparation was employed by oligo-dT selection assay by using NEBNext® Ultra RNA Library Prep Kit for Illumina® (NEB) and sequenced on an Illumina NovaSeq platform (Berry Genomics, China).

Three RNA-seq datasets from cultured P0 DRG neurons were aligned to rat genome assembly (RGSC Rno5\_5.0/rn5) using HISAT2 ([Kim et al., 2015](#)). The alignments were passed to StringTie ([Pertea et al., 2015](#)) for transcript assemblies, followed by StringTie merge function with annotations from Ensembl (release 79) and RefSeq (updated at 2018/08/27).

A series of filters were used to ensure the reliable identification of lincRNAs from our datasets. First, all transcripts with a single exon and less than 200 nucleotides were removed. Additionally, the transcripts that had any overlap with annotated protein-coding genes, pseudogenes or small RNAs in Ensembl were excluded. Second, the coding potential of transcripts was estimated in three ways, including CPAT (version 2.0.0) ([Wang et al., 2013](#)), CPC2 (version 0.1) ([Kang et al., 2017](#)) and PfamScan (version 1.6) ([Eddy, 2011](#)). Finally, total 3,032 new transcripts passed above filters and 69 of known lincRNAs from Ensembl were kept lincRNAs for subsequent analysis. The expression level of all lincRNAs was recalculated using FPKM from featureCounts ([Liao et al., 2014](#)). Together, among 3,101 lincRNAs of identified lincRNAs in P0 DRG neurons, 462 of highly expressed lincRNAs ( $\text{FPKM} \geq 1$  and splicing site coverage  $\geq 1$ ) were selected. The list of expressed lincRNAs was provided in [Table S1](#).

### Statistical analysis

All data are presented as the mean  $\pm$  SEM. Statistical analyses were performed using unpaired t tests to evaluate effects in single-factor experiments and two-way ANOVA test to determine the effects of each variables in two-factor experiments (GraphPad Software). Differences were considered significant at  $p < 0.05$ .

**Supplemental information**

**Axon-enriched lincRNA *ALAE* is required  
for axon elongation via regulation  
of local mRNA translation**

**Manyi Wei, Jiansong Huang, Guo-Wei Li, Bowen Jiang, Hong Cheng, Xiaoyan Liu, Xingyu  
Jiang, Xu Zhang, Li Yang, Lan Bao, and Bin Wang**

## **Supplemental Information**

### **Axon-enriched lincRNA *ALAE* is required for axon elongation via regulation of local mRNA translation**

Manyi Wei, Jiansong Huang, Guo-Wei Li, Bowen Jiang, Hong Cheng, Xiaoyan Liu,  
Xingyu Jiang, Xu Zhang, Li Yang, Lan Bao, Bin Wang

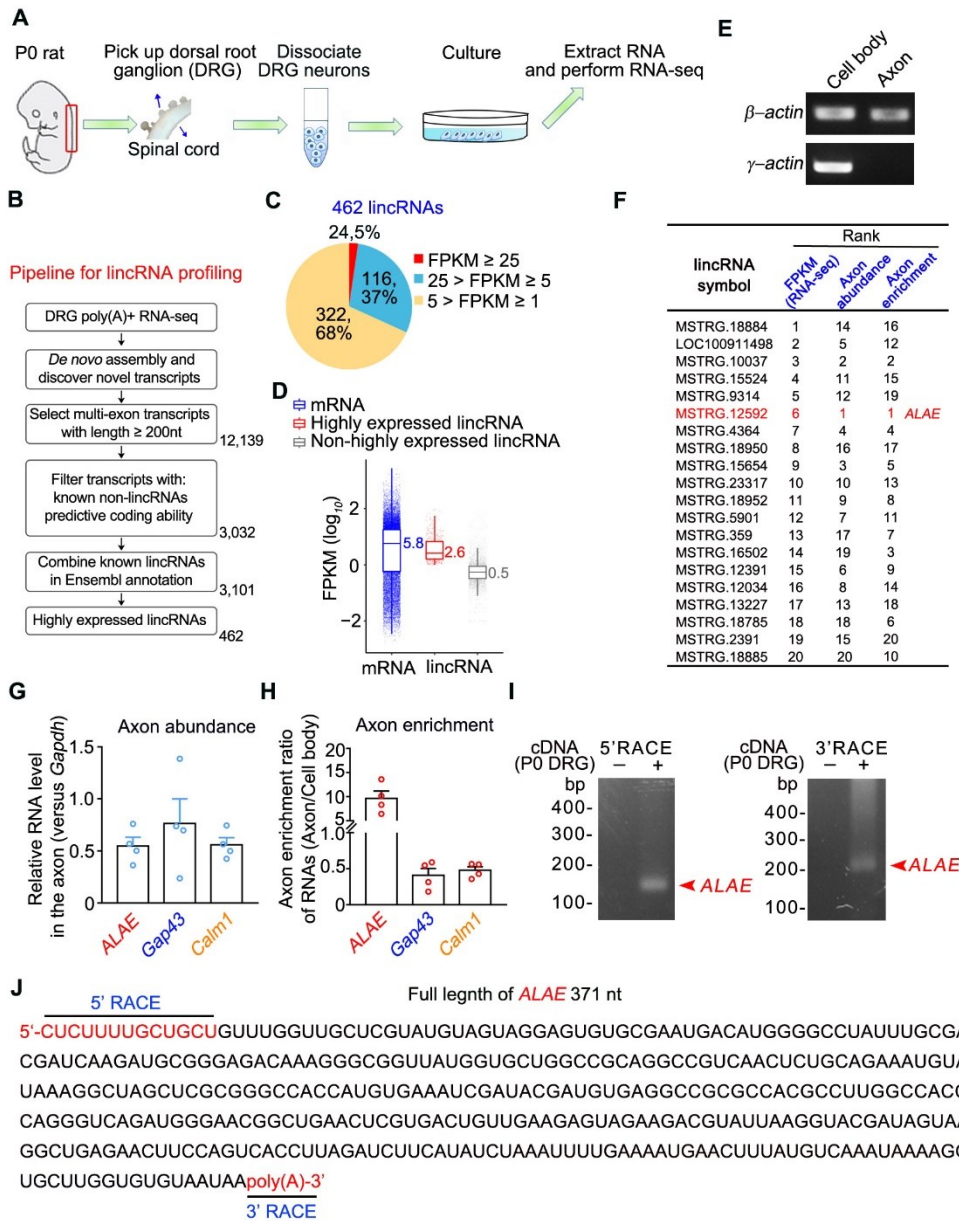


**Figure S1. Related to Figure 1, Characterization of axon-enriched ALAE in DRG**

## neurons

(A) Flowchart of cultured P0 DRG neurons for RNA-seq. P0 DRGs were picked up and dissociated. After cultured for 48 h, RNA of P0 DRG neurons was extracted and performed by high throughput RNA-seq as well as bioinformatic analysis to profile lincRNAs.

(B) Pipeline of profiling lincRNAs in cultured P0 DRG neurons.

(C) Abundance distribution of 462 highly expressed lincRNAs ( $\text{FPKM} \geq 1$ ) from total expressed 3101 lincRNAs based on RNA-seq of cultured P0 DRG neurons.

(D) Plot showing the expression of mRNAs and lincRNAs from RNA-seq of cultured P0 DRG neurons.

(E) RT-PCR results showed that  $\gamma\text{-actin}$  was distributed in the cell bodies of P0 DRG neurons at 7 DIV in the microfluidic chamber, whereas  $\beta\text{-actin}$  was observed in both cell bodies and axons.

(F) The ranking list showed that *ALAE* was the most abundant and enriched lincRNA among top 20 lincRNAs in the axons of DRG neurons by qPCR.

(G and H) qPCR analysis showed that the abundance of *ALAE* in the axons was equivalent to *Gap43* and *Calm1* mRNAs (G) and the enrichment of *ALAE* in the axons was much higher than *Gap43* and *Calm1* mRNAs (H). The results are presented as mean  $\pm$  SEM ( $n = 4$ ).

(I) 5'RACE (Left) and 3'RACE (Right) PCR analyzed 5' and 3' ends of *ALAE* in P0 DRG, respectively. The arrow indicated the DNA fragment cloned and sequenced to map the 5' or 3'-end sequence of *ALAE*.

(J) The full sequence of *ALAE* by 5'RACE and 3'RACE.

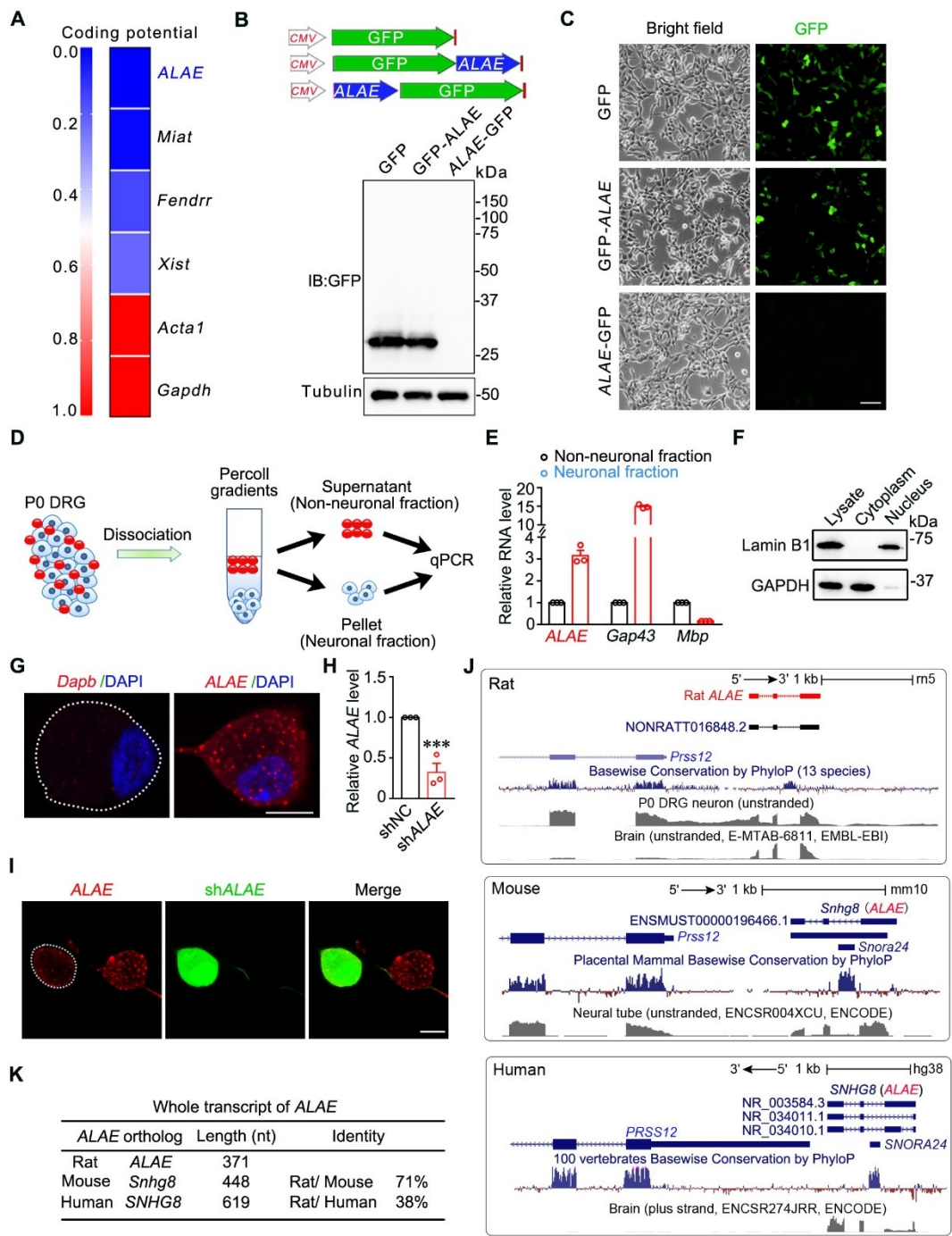


**Figure S2. Related to Figure 1, ALAE is a neuron-enriched and highly conserved lincRNA**

(A) Computational result analyzed by CPC2 software showed that *ALAE* has no ability in protein translation. *Miat* and *Fendrr* are known lncRNAs without coding ability. *Gapdh* and *Actb1* are coding genes.

(B and C) Schematic of GFP, GFP-*ALAE* and *ALAE*-GFP plasmids (B, Upper).

Representative immunoblots displayed the similar molecular weight of GFP-*ALAE* as GFP (B, Down) and fluorescent images showed that *ALAE*-GFP was not expressed in cultured HKE293 cells (C). Tubulin served as a loading control. Scale bar, 50  $\mu$ m.

(D and E) Flowchart for the purification of neuronal fraction (D). Purified P0 DRG neurons were separated from dissociated DRG cells by Percoll gradients. qPCR analysis showed that *ALAE* was relatively more enriched in the neuronal fraction marked by *Gap43* mRNA, a protein exclusively distributed in neuronal fraction (E), but not *Mbp* mRNA, a marker of Schwann cells.

(F) Combination of biochemical separation with immunoblotting showed that lamin B1 was distributed in the nuclear fraction, whereas GAPDH was exclusively observed in the cytoplasmic fraction of cultured P0 DRG neurons.

(G) Representative images of SmFISH showed that *ALAE* was localized in the cultured P0 DRG neurons, whereas a negative control *Dapb* did not display obvious fluorescent signals. Scale bar, 10  $\mu$ m.

(H) qPCR analysis showed the efficiently shRNA-mediated knockdown of *ALAE* in cultured P0 DRG neurons. The results are presented as the mean  $\pm$  SEM ( $n = 3$ ). \*\*\*,  $P < 0.001$  versus shNC.

(I) Representative images of SmFISH showed that *ALAE* was decreased in neurons expressing GFP (sh*ALAE*) compared to those neurons without expressing GFP. Scale bar, 10  $\mu$ m.

(J) Conservation analysis showed that *ALAE* is conserved among rat, mouse and human.

*ALAE* is genomically conserved in the downstream of *Prss12* with opposite direction in rat, mouse and human. Additionally, *Snora24* genomically overlaps with introns of *ALAE* in rat, mouse and human. The orthologs of *ALAE* in human and mouse are named as *SNHG8* and *Snhg8* expressed in the brain of human and neural tube of mice. RNA-seq datasets from brain were taken from EMBL-EBI and ENCODE: E-MATB-6811(Rat); ENCSR004XCU (Mouse); ENCSR274JRR (Human).

(K) Analysis of the length and sequence identity of *ALAE* orthologs among human, mouse and rat.

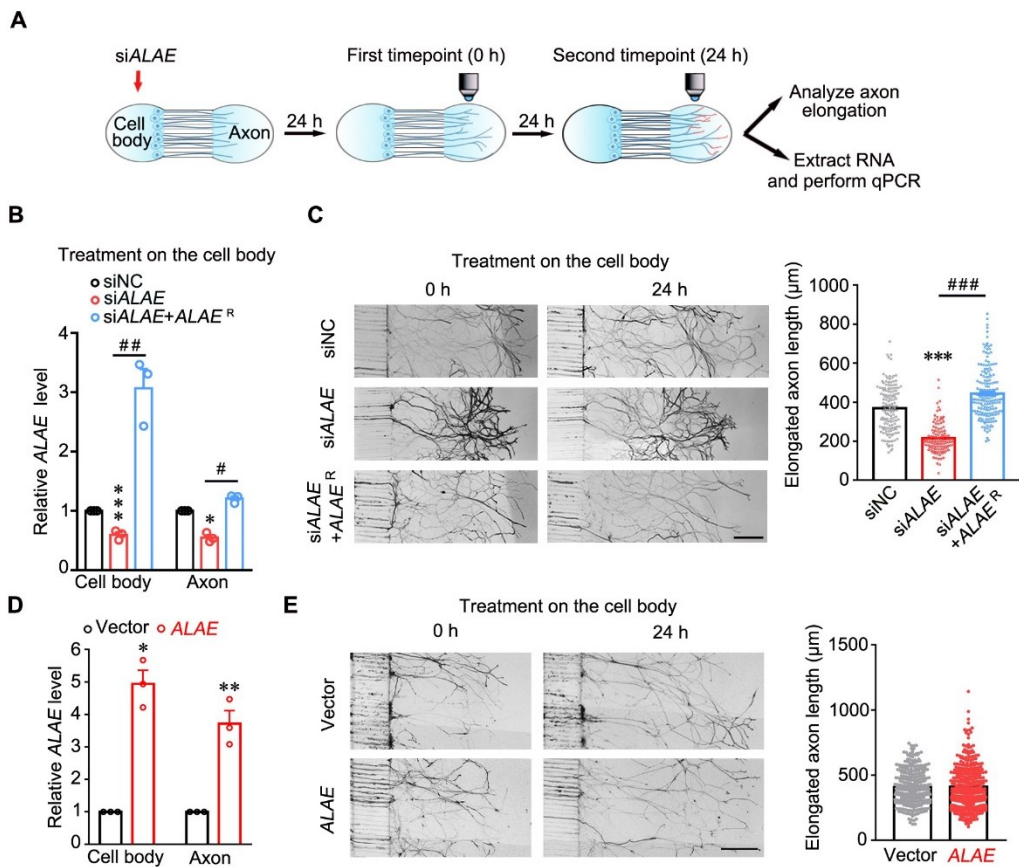


Figure S3, Wei & Huang, 2021

**Figure S3. Related to Figure 1, Knockdown of *ALAE* in the cell body compartment reduces axon elongation, whereas overexpression of *ALAE* doesn't affect axon elongation**

(A) The flowchart for detection of axon elongation by knockdown of *ALAE* in the cell body compartment of microfluidic chamber. After application of si*ALAE* in cell body compartment for 24 h, the elongated axon length will be traced and measured for another 24 h. The expression level of *ALAE* in the cell bodies or axons were analyzed by qPCR.

(B) qPCR analysis showed the expression level of *ALAE* in the cell bodies and axons after either knockdown or coexpression of *ALAE*<sup>R</sup> in the cell body compartment of DRG

neurons. The results are presented as the mean  $\pm$  SEM (siNC, n = 140; si*ALAE*, n = 115; si*ALAE+ALAE<sup>R</sup>*, n = 184). \*\*\*P < 0.001 versus siNC and ## P < 0.01, ### P < 0.001 versus indicated.

(C) Representative images (Left) and quantitative data (Right) showed that knockdown of *ALAE* in the cell body compartment decreased axon elongation and coexpression of *ALAE<sup>R</sup>* in the cell bodies largely rescued decreased axon elongation induced by si*ALAE*. The results are presented as the mean  $\pm$  SEM (n = 3). \*\* P < 0.01 versus siNC and ### P < 0.001 versus indicated. Scale bar, 300  $\mu$ m.

(D) qPCR analysis showed that the expression level of *ALAE* in the cell bodies and axons were increased after overexpression of *ALAE* in the cell bodies of DRG neurons. The results are presented as the mean  $\pm$  SEM (n = 3). \*P < 0.05, \*\*P < 0.01 versus vector.

(E) Representative images (Left) and quantitative data (Right) showed that overexpression of *ALAE* in the cell body compartment didn't affect axon elongation. The results are presented as the mean  $\pm$  SEM (Vector, n = 305; *ALAE*, n = 354). Scale bar, 300  $\mu$ m.

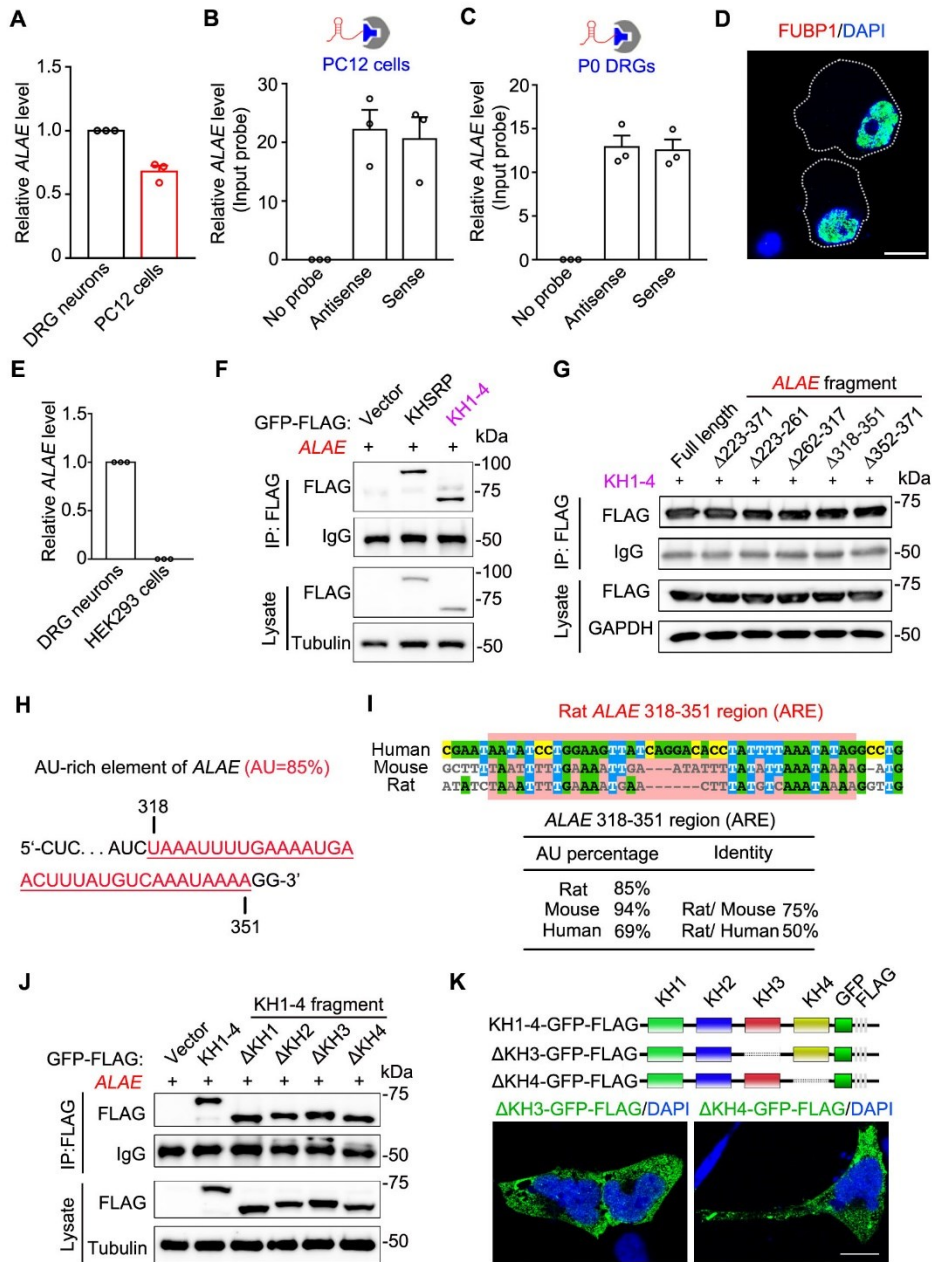


**Figure S4. Related to Figures 2 and 3, ALAE associates with KHSRP through AREs in DRG neurons**

(A) qPCR analysis showed that the expression of *ALAE* in PC12 cells displayed similar level to cultured P0 DRG neurons. The results are presented as the mean  $\pm$  SEM ( $n = 3$ ).

(B and C) qPCR analysis showed the similar level of *ALAE* pulled down by biotinylated antisense (negative control) and sense transcripts of *ALAE* in PC12 cells (B) and P0 DRGs (C). The results are presented as the mean ± SEM (n = 3).

(D) Representative immunofluorescence images showed that FUBP1 was exclusively distributed in the nucleus of cultured P0 DRG neurons. Scale bar, 10 μm.

(E) qPCR analysis showed that *ALAE* was almost absent in HEK293 cells compared to cultured P0 DRG neurons. The results are presented as the mean ± SEM (n = 3).

(F) Representative immunoblots showing the products of immunoprecipitation by FLAG in HEK293 cells expressing KHSRP-GFP-FLAG or KH1-4-GFP-FLAG. Tubulin or IgG served as the loading control.

(G) Representative immunoblots showing the products of immunoprecipitation by FLAG in HEK293 cells expressing KH1-4-GFP-FLAG and fragments of *ALAE*. Tubulin or IgG served as the loading control.

(H) The 318-351 nt of *ALAE* is an AU-rich element (AREs). The 318-351 nt of *ALAE* (Highlighted in red) contains 85% AU residues.

(I) The sequence identity analysis showed that the AREs of *ALAE* 318-351 region is highly conserved among rodents and human.

(J) Representative immunoblots showing the products of immunoprecipitation by FLAG in HEK293 cells expressing KH1-4-GFP-FLAG fragments with *ALAE*. Tubulin or IgG served as the loading control.

(K) Schematic of KH1-4 truncations (Upper). Representative immunofluorescent images (Down) showed that the truncation deleting either KH3 or KH4 of KH1-4-GFP

exhibited cytoplasmic localization. Scale bar, 10  $\mu\text{m}$ .

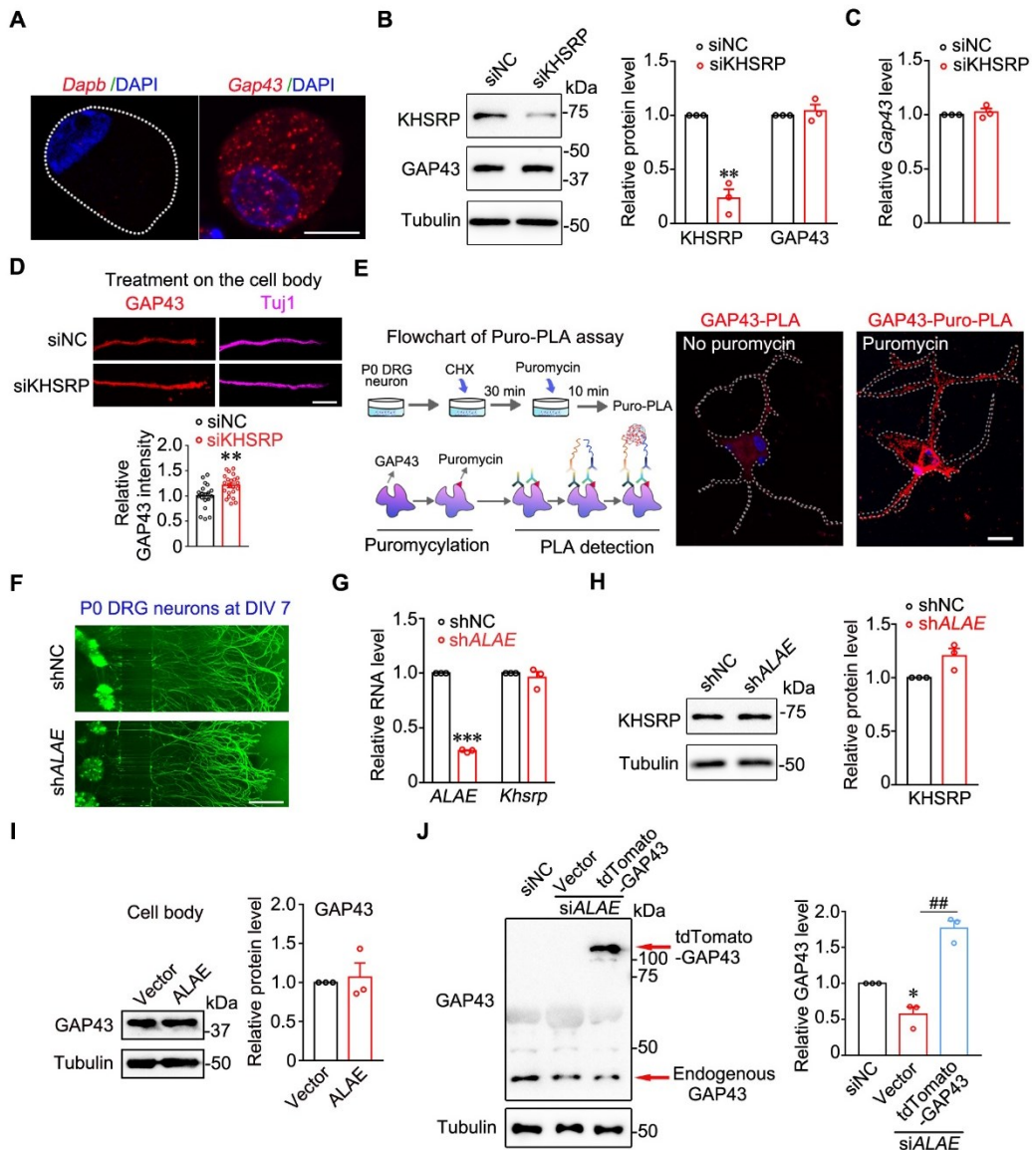


**Figure S5. Related to Figures 4 and 5, ALAE downregulation doesn't affect the mRNA and protein levels of KHSRP**

(A) Representative images of SmFISH showed that *Gap43* mRNA was localized in the cultured P0 DRG neurons, whereas *Dapb* mRNA as a negative control was not detected by obvious fluorescent signals. Scale bar, 10  $\mu$ m.

(B) Representative immunoblots (Left) and quantitative data (Right) showed that the amounts of GAP43 were not affected by KHSRP knockdown in cultured P0 DRG neurons. The results are presented as the mean  $\pm$  SEM ( $n = 3$ ).

(C) qPCR analysis showed that *ALAE* was not affected by KHSRP knockdown in cultured P0 DRG neurons. The results are presented as the mean ± SEM (n = 3).

(D) Representative images (Left) and quantitative data (Right) showed that knockdown of KHSRP in the cell body compartment increased the intensity of GAP43 in axons in the microfluidic-cultured P0 DRG neurons. The results are presented as mean ± SEM (siNC, n = 19; siKHSRP, n = 22). \*\*P < 0.01 versus siNC. Scale bar, 10 μm.

(E) Flowchart for Puro-PLA assay (Left). Representative images showed that newly synthesized GAP43 was visualized by Puro-PLA assay in cultured P0 DRG neurons (Right). Scale bar, 20 μm.

(F) Representative images showing highly efficient infection of AAV-shNC-GFP and AAV-sh*ALAE*-GFP in the cell bodies and axons of microfluidic-cultured P0 DRG neurons at DIV 7. shNC, negative control. Scale bar, 300 μm.

(G) qPCR analysis showed that *Khsrp* mRNA was not affected by infection with AAV-sh*ALAE*. The results are presented as mean ± SEM (n = 3).

(H) Representative immunoblots (Left) and quantitative data (Right) showed that the amount of KHSRP was not affected by infection with AAV-sh*ALAE* in cultured P0 DRG neurons. The results are presented as the mean ± SEM (n = 3).

(I) Representative immunoblots (Left) and quantitative data (Right) showed that the protein level of GAP43 was not influenced by *ALAE* overexpression in the cell body compartment of cultured P0 DRG neurons. The results are presented as mean ± SEM (n = 3).

(J) Representative immunoblots (Left) and quantitative data (Right) showed that

coexpression of tdTomato-GAP-43 fully rescued the decreased amount of GAP43 by si*ALAE* in the cell body compartment of microfluidic-cultured P0 DRG neurons. The results are presented as the mean  $\pm$  SEM ( $n = 3$ ). \* $P < 0.05$  versus siNC and \*\* $P < 0.01$  versus indicated.

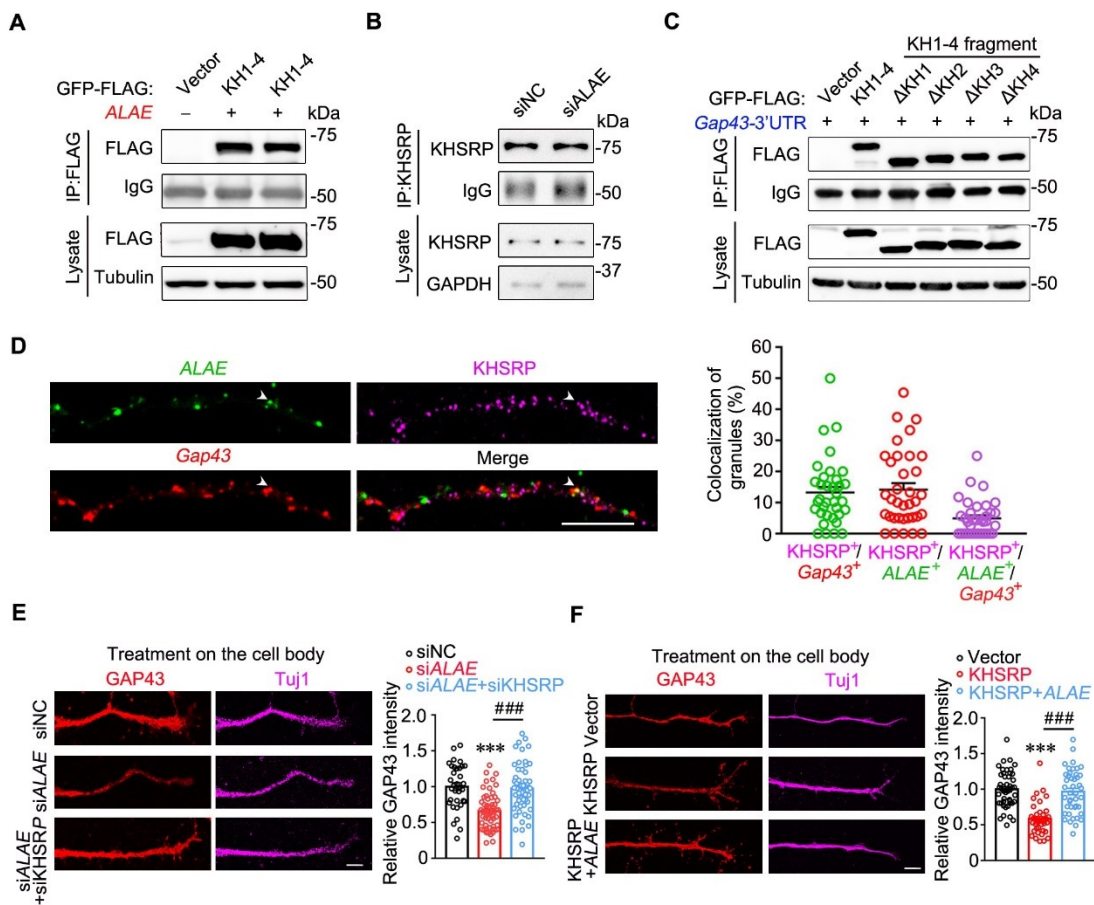


**Figure S6. Related to Figure 6, ALAE impedes the association between KHSRP and *Gap43* mRNA**

(A) Representative immunoblots showing the products of immunoprecipitation by FLAG in HEK293 cells expressing KH1-4-GFP-FLAG with *Gap43-3'UTR* in the absence or presence of *ALAE*. Tubulin or IgG served as the loading control.

(B) Representative immunoblots showing the products of immunoprecipitation by KHSRP after siRNA-mediated knockdown of *ALAE* in PC12 cells. GAPDH or IgG served as the loading control.

(C) Representative immunoblots showing the products of immunoprecipitation by FLAG in HEK293 cells expressing KH1-4 fragments with *Gap43-3'UTR*. Tubulin or IgG served as the loading control.

(D) Representative images (Left) and quantitative data (Right) showed that *ALAE* (Green), *Gap43* mRNA (Red) and KHSRP (Purple) were rarely co-localized in the axons of cultured P0 DRG neurons. The results are presented as mean ± SEM (n = 35).

Scale bar, 10  $\mu$ m.

(E) Representative images (Left) and quantitative data (Right) showed that the reduced intensity of GAP43 in the axons due to knockdown of *ALAE* in the cell body compartment were completely rescued by knockdown of KHSRP in microfluidic-cultured P0 DRG neurons. The results are presented as mean ± SEM (siNC, n = 34; si*ALAE*, n=58; si*ALAE*+ siKHSRP, n = 57). \*\*\* P < 0.001 versus siNC and ### P < 0.001 versus indicated. Scale bar, 10  $\mu$ m.

(F) Representative images (Left) and quantitative data (Right) showed that the reduced intensity of GAP43 in the axons caused by overexpression of KHSRP in the cell body compartment were completely rescued by coexpression of *ALAE* in microfluidic-cultured P0 DRG neurons. The results are presented as mean ± SEM (Vector, n = 46; KHSRP, n=40; KHSRP+ *ALAE*, n = 43). \*\*\* P < 0.001 versus Vector and ### P < 0.001 versus indicated. Scale bar, 10  $\mu$ m.

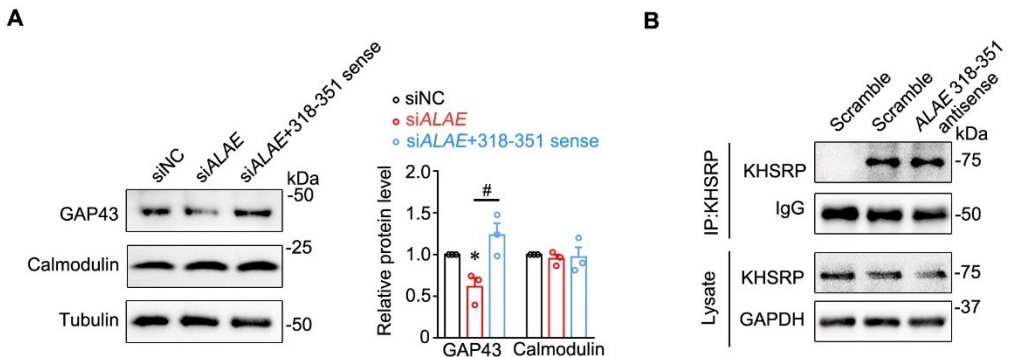


**Figure S7. Related to Figure 7, ALAE3 18-351 is sufficient for the function of ALAE on GAP43 in cultured P0 DRG neurons**

(A) Representative immunoblots (Left) and quantitative data (Right) showed that the reduced level of GAP43 after knockdown of *ALAE* in cultured P0 DRG neurons was fully rescued by coexpression of *ALAE318-351* sense fragment. Calmodulin was used as a control that was not affected by treatment. Tubulin served as the loading control. The results are presented as the mean  $\pm$  SEM ( $n = 3$ ). \*  $P < 0.05$  versus siNC and #  $P < 0.05$  versus indicated.

(B) Representative immunoblots showing the immunoprecipitates by KHSRP after application of *ALAE* 318-351 antisense in cultured P0 DRG neurons. GAPDH or IgG served as the loading control.